Medicago truncatula Natural Resistance-Associated Macrophage Protein1 Is Required for Iron Uptake by Rhizobia-Infected Nodule Cells[1][OPEN]

Manuel Tejada-Jiménez[2], Rosario Castro-Rodríguez[2], Igor Kryvoruchko[3], M. Mercedes Lucas, Michael Udvardi, Juan Imperial, and Manuel González-Guerrero*

Centro de Biotecnología y Genómica de Plantas, Campus de Montegancedo, Universidad Politécnica de Madrid, 28223 Madrid, Spain (M.T.-J., R.C.-R., J.I., M.G.-G.); Plant Biology Division, The Samuel Roberts Noble Foundation, Ardmore, Oklahoma 73401 (I.K., M.U.); Instituto de Ciencias Agrarias, Consejo Superior de Investigaciones Científicas, 28006 Madrid, Spain (M.M.L.); and Consejo Superior de Investigaciones Científicas, 28006 Madrid, Spain (J.I.)

Iron is critical for symbiotic nitrogen fixation (SNF) as a key component of multiple ferroproteins involved in this biological process. In the model legume *Medicago truncatula*, iron is delivered by the vasculature to the infection/maturation zone (zone II) of the nodule, where it is released to the apoplast. From there, plasma membrane iron transporters move it into rhizobia-containing cells, where iron is used as the cofactor of multiple plant and rhizobial proteins (e.g. plant leghemoglobin and bacterial nitrogenase). *MtNramp1* (*Medtr3g088460*) is the *M. truncatula* Natural Resistance-Associated Macrophage Protein family member, with the highest expression levels in roots and nodules. Immunolocalization studies indicate that MtNramp1 is mainly targeted to the plasma membrane. A loss-of-function *nramp1* mutant exhibited reduced growth compared with the wild type under symbiotic conditions, but not when fertilized with mineral nitrogen. Nitrogenase activity was low in the mutant, whereas exogenous iron and expression of wild-type *MtNramp1* in mutant nodules increased nitrogen fixation to normal levels. These data are consistent with a model in which MtNramp1 is the main transporter responsible for apoplastic iron uptake by rhizobia-infected cells in zone II.

SNF is carried out by the endosymbiosis between legumes and diazotrophic bacteria called rhizobia (van Rhijn and Vanderleyden, 1995). Detection of rhizobial nodulation (Nod) factors by the legume plant results in curling of a root hair around the rhizobia and development of an infection thread that will deliver the rhizobia to the developing root nodule primordium, which is also triggered by Nod factors (Kondorosi et al., 1984; Brewin, 1991; Oldroyd, 2013). Rhizobia are eventually released into the cytoplasm of host plant cells via endocytosis, resulting in an organelle-like structure known as the symbiosome, which consists of bacteria surrounded by a plant membrane called the symbiosome membrane (SM; Roth and Stacey, 1989; Vasse et al., 1990). Rhizobia within symbiosomes eventually differentiate into nitrogen-fixing bacteroids that produce and export ammonium to the plant for assimilation (Vasse et al., 1990).

Two main developmental programs for nodulation have been described (Sprent, 2007). In the determinate type, e.g. in soybean (*Glycine max*), the nodule meristem is active only transiently, which gives rise to a spherical nodule. In the indeterminate nodules, e.g. in alfalfa (*Medicago sativa*) and pea (*Pisum sativum*), the meristem(s) remain active for much longer, resulting in cylindrical and/or branched nodules of indeterminate morphology. Indeterminate nodules can be divided in spatiotemporal zones that facilitate the study of the nodulation process. At least four zones are observed in a mature indeterminate nodule (Vasse et al., 1990). Zone I is the meristematic region that drives nodule growth. In zone II, rhizobia are released from the infection thread and differentiate into bacteroids. Zone III is the site of nitrogen fixation. Finally, Zone IV is the senescence zone, where bacteroids are degraded and nutrients are recycled. Some authors describe two more zones: the interzone, a transition zone between zones II and III (Vasse et al., 1990; Roux et al., 2014), and zone V, where saprophytic rhizobia live on the nutrients released by senescent cells (Timmers et al., 2000).

Nodulation and nitrogen fixation are tightly regulated processes (for review, see Oldroyd, 2013; Udvardi and Poole, 2013; Downie, 2014) and require a relatively large

[1] This work was supported by the Spanish Ministry of Economy and Competitiveness (grant no. AGL–2012–32974 to M.G.-G. and Formación del Personal Investigador fellowship no. BES–2013–062674 to R.C.-R.), a Marie Curie International Reintegration grant (grant no. IRG–2010–276771 to M.G.-G.), a European Research Council Starting grant (grant no. ERC–2013–StG–335284 to M.G.-G.), and a Ramón y Cajal fellowship (no. RYC–2010–06363 to M.G.-G.).

[2] These authors contributed equally to the article.

[3] Present address: Kafkas Üniversitesi, Mühendislik Mimarlık Fakültesi, Biyomühendislik Bölümü, 36100 Kars, Turkey.

* Address correspondence to manuel.gonzalez@upm.es.

The author responsible for distribution of materials integral to the findings presented in this article in accordance with the policy described in the Instructions for Authors (www.plantphysiol.org) is: Manuel González-Guerrero (manuel.gonzalez@upm.es).

[OPEN] Articles can be viewed without a subscription.

www.plantphysiol.org/cgi/doi/10.1104/pp.114.254672

supply of nutrients from the host: photosynthates, macronutrients such as phosphate and sulfate, amino acids, at least prior to nitrogen fixation, and metal micronutrients (Udvardi and Poole, 2013). Among the latter, iron is one of the most critical (Brear et al., 2013; González-Guerrero et al., 2014). The activity of some of the most abundant and important enzymes in SNF directly depends on iron as cofactor. Nitrogenase, the enzyme directly responsible for nitrogen fixation, needs iron-sulfur clusters and an iron-molybdenum cofactor to reduce N_2 (Miller et al., 1993). The hemoprotein leghemoglobin, which controls O_2 levels in the nodule (Ott et al., 2005), represents around 20% of total nodule protein (Appleby, 1984). Similarly, different types of superoxide dismutase, including an Fe-superoxide dismutase, control the free radicals produced during SNF (Rubio et al., 2007). Other ferroproteins are involved in energy transduction and recycling related to the nitrogen fixation process (Ruiz-Argüeso et al., 1979; Preisig et al., 1996).

Despite its importance, iron is a growth-limiting nutrient for plants in most soils (Grotz and Guerinot, 2006), especially in alkaline soils. As a result, iron deficiency is prevalent in plants and hampers crop production and human health (Grotz and Guerinot, 2006; Mayer et al., 2008). This is even more so when legumes are nodulated (Terry et al., 1991; Tang et al., 1992). The relatively high iron demand of nodules can trigger the iron deficiency response, i.e. increase in iron reductase activities in the root epidermis and acidification of the surrounding soil (Terry et al., 1991; Andaluz et al., 2009). Consequently, knowing how iron homeostasis is maintained in nodulated legumes, including how this micronutrient is delivered to the nodule, is important for understanding and improving SNF.

Taking advantage of state-of-the-art metal visualization methods, the pathway for iron delivery to the nodule has been elucidated (Rodríguez-Haas et al., 2013). Synchrotron-based x-ray fluorescence studies on *Medicago truncatula* indeterminate nodules indicate that most of the iron is delivered by the vasculature to the apoplast of zone II. In zone III, iron is mostly localized within bacteroids. Therefore, a number of transporters must exist that move iron through the plasma membrane of plant cells and the SM of infected cells. Several transporters have been hypothesized to mediate iron transport through the SM. Soybean Divalent Metal Transporter1 (GmDMT1) is a nodule-induced Natural Resistance-Associated Macrophage Protein (Nramp) that was found in the soybean SM using specific antibodies (Kaiser et al., 2003). However, biochemical studies on Nramp transporters suggest that they transport substrates into the cytosol (Nevo and Nelson, 2006), rather than outwards or into symbiosomes. More recently, the study of *stationary endosymbiont nodule1* (*sen1*) mutants in *Lotus japonicus* indicated that SEN1, a yeast (*Saccharomyces cerevisiae*) Cross Complements CSG1/Arabidopsis (*Arabidopsis thaliana*) Vacuolar Iron Transporter1 homolog, could play a role in delivering iron across the SM (Hakoyama et al., 2012), albeit this is merely based on the mutant plant phenotype and the role of members of this family in other organisms.

Very little is known about the molecular identity of transporters that mediate iron uptake from the nodule apoplast. Based on known plant metal transporters and their biochemistry, the most likely candidates are members of the Nramp and Zinc-Regulated Transporter1, Iron-Regulated Transporter1-Like Protein (ZIP) families, because these can transport divalent metals into the cytosol (Vert et al., 2002; Nevo and Nelson, 2006). Moreover, given that the expression of at least one Nramp transporter (GmDMT1) is activated by nodulation (Kaiser et al., 2003), it is possible that members of this family might mediate iron uptake into rhizobia-containing cells. Nramp transporters are ubiquitous divalent transition metal importers (Nevo and Nelson, 2006). Phenotypical and electrophysiological studies indicate that they have a wide range of possible biological (Fe^{2+}, Mn^{2+}, Zn^{2+}, Cu^{2+}, Co^{2+}, and Ni^{2+}) and nonbiological (Pb^{2+} and Cd^{2+}) substrates (Belouchi et al., 1997; Curie et al., 2000; Thomine et al., 2000; Mizuno et al., 2005; Rosakis and Köster, 2005; Cailliatte et al., 2009). In plants, Nramp transporters have been associated with a number of biological roles, such as Fe^{2+} and Mn^{2+} uptake from soil (Curie et al., 2000; Cailliatte et al., 2010), Mn^{2+} long-distance trafficking (Yamaji et al., 2013), metal remobilization during germination (Lanquar et al., 2005), Cd^{2+} and Ni^{2+} tolerance (Mizuno et al., 2005; Cailliatte et al., 2009), and the immune response (Segond et al., 2009), in addition to participating in SNF (Kaiser et al., 2003).

In this study, *M. truncatula MtNramp1* (*Medtr3g088460*) was identified as the Nramp transporter gene expressed at the highest levels in nodules. MtNramp1 protein was localized in the plasma membrane of nodule cells in zone II, where the expression reached its maximum. Its role in iron uptake and its importance for SNF were established using a loss-of-function mutant, *nramp1-1*. This work adds to our understanding of how apoplastic metals are imported into nodule cells.

RESULTS

MtNramp1 Transcription Is Induced during Nodule Development

Inspection of the M. *truncatula* genome sequence revealed eight genes with similarity to Nramp transporters. Seven of them, *MtNramp1* to *MtNramp7* (*Medtr3g088460*, *Medtr3g088440*, *Medtr2g104990*, *Medtr3g102620*, *Medtr5g016270*, *Medtr8g028050*, and *Medtr4g095075*, respectively) are similar to Nramp transporters throughout their sequence. The eighth gene (*Medtr004150030*) is an Arabidopsis *Ethylene Insensitive2* homolog that shows a very high sequence similarity to Nramp transporters only in its C terminus. Sequence comparison of the seven MtNramp sequences with known plant Nramp transporters showed that they cluster in two different groups (Fig. 1A). Nodule-specific Nramp transporter GmDMT1 from soybean clusters in the same branch together with MtNramp5 and MtNramp7. MtNramp1 structure was modeled using *Staphylococcus capitis* DMT structure (Ehrnstorfer et al., 2014; Fig. 1B). The predicted

model had a high degree of homology with ScDMT1, sharing the same four metal-coordinating amino acids (D60, N63, A232, and M235 in MtNramp1). The predicted structure also shows the 11 transmembrane domains characteristic of Nramp transporters.

Expression levels of the seven putative transporter genes in 28-d-postinoculation (dpi) nodules, roots fertilized with nitrogen, and denodulated roots (stripped of nodules) were measured by quantitative reverse transcription-PCR. *MtNramp1* showed the highest transcript levels in denodulated roots of the seven genes studied (Fig. 2A). None of these genes had significantly higher levels of expression in nodules than in roots (Fig. 2B; Supplemental Fig. S1). However, *MtNramp1* was the most highly expressed of the seven Nramp-like genes in nodules (Fig. 2C), indicating its preeminent role in these organs.

MtNramp1 Is an Iron and Manganese Importer

MtNramp1 substrate and direction of transport were determined by complementation of yeast mutants affected in metal transport. The closest *MtNramp1* homolog in yeast is the manganese importer *Suppressor of Mitochondria Import Function1* (*SMF1*; *YOL122C*). Mutation of *SMF1* results in loss of the ability to grow on manganese-depleted medium (Supek et al., 1996; Fig. 3A). To determine whether *MtNramp1* is functionally equivalent to *SMF1*, its complementary DNA (cDNA) was cloned into yeast pYPGE15 vector under the control of the yeast constitutive phosphoglycerate kinase promoter and transformed in the *smf1* mutant strain. The transformed strain possessed the ability to grow on low manganese, like the wild-type strain (Fig. 3A).

Nramp transporters have also been implicated in iron import, either from the cell exterior or from an organelle (Curie et al., 2000; Forbes and Gros, 2001). Given the importance of iron in SNF, MtNramp1 iron transport capability was tested by assessing its ability to complement the yeast *Fe Transport3* (*fe3*)/*fet4* double mutant. FET3 (YMR058W) is a multicopper ferroxidase involved in high-affinity iron uptake (Askwith et al., 1994), while FET4 (YMR319C) is a low-affinity iron importer (Dix et al., 1994). The double mutant has a severe impairment in iron uptake, requiring higher iron levels in the medium and a more acidic environment to increase this micronutrient mobility and availability. The expression of *MtNramp1* in the *fet3*/*fet4* background

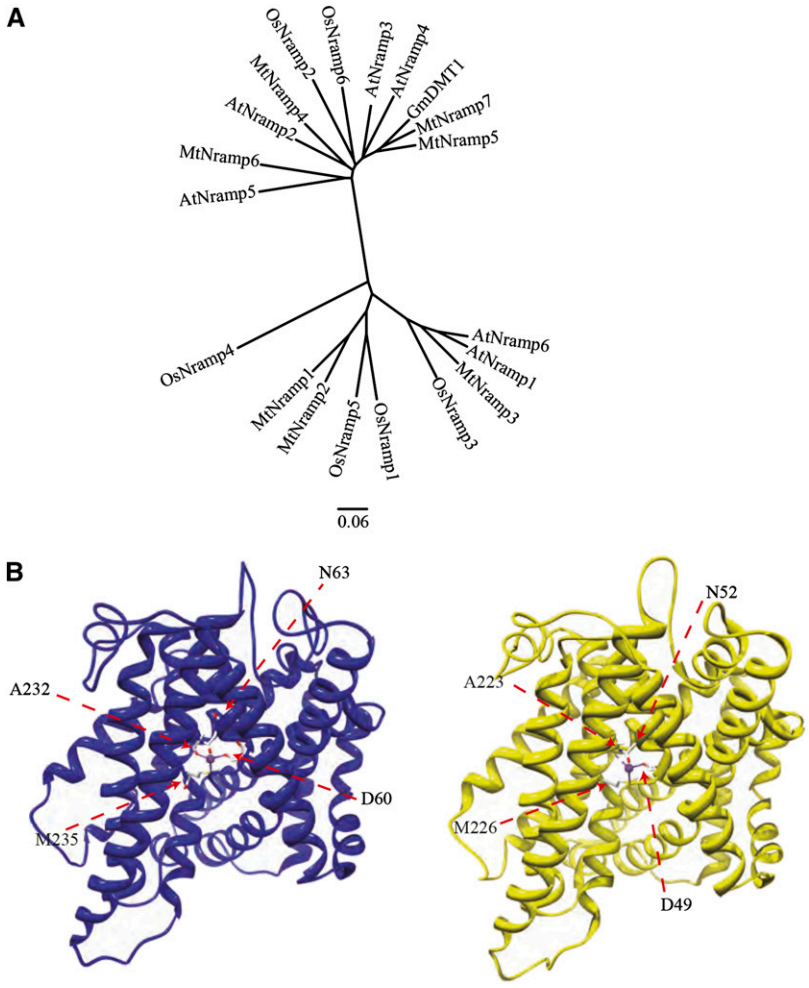

Figure 1. *M. truncatula* Nramp family. A, Unrooted tree of the *M. truncatula* Nramp family transporters MtNramp1 to MtNramp7 (*Medtr3g088460*, *Medtr3g088440*, *Medtr2g104990*, *Medtr3g102620*, *Medtr5g016270*, *Medtr8g028050*, and *Medtr4g095075*, respectively) and representative plant Nramp homologs AtNramp1 (*At1g80830*), AtNramp2 (*At1g47240*), AtNramp3 (*At2g23150*), AtNramp4 (*At5g67330*), AtNramp5 (*At4g18790*), AtNramp6 (*At1g15960*), OsNramp1 (*Os07g0258400*), OsNramp2 (*Os03g0208500*), OsNramp3 (*Os06g0676000*), OsNramp4 (*Os01g0503400*), OsNramp5 (*Os07g0257200*), OsNramp6 (*Os12g0581600*), and GmDMT1 (*Glyma17g18010*). B, Tertiary structure modeling of MtNramp1 (blue) and template *S. capitis* DMT1 (Protein Data Bank Identification: 4WGW, yellow). Positions of metal coordinating amino acids are indicated.

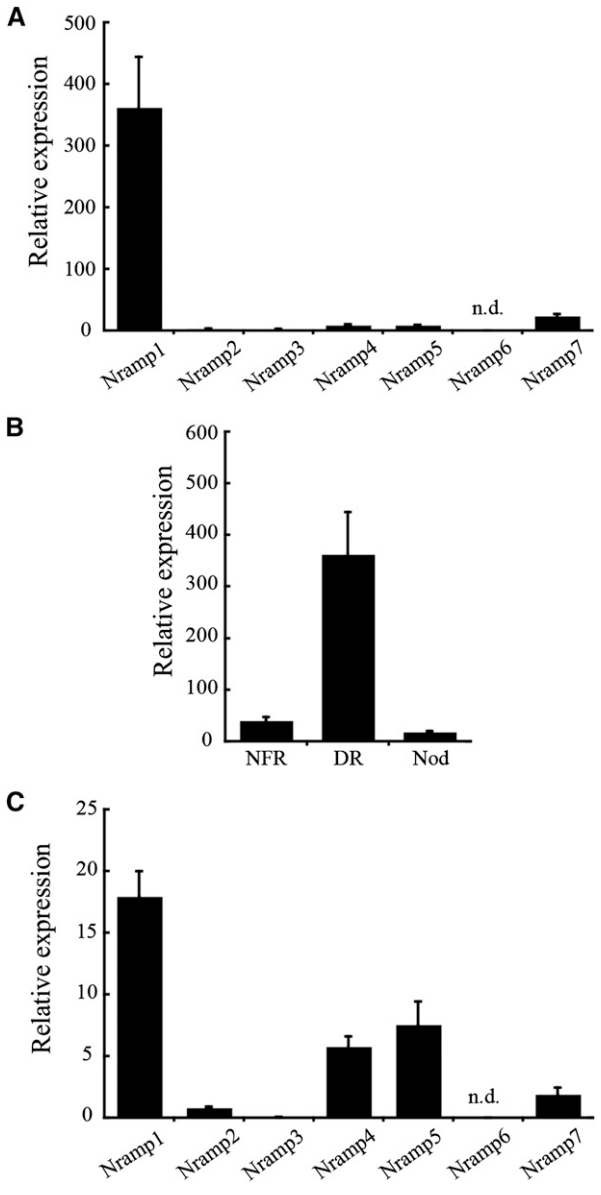

Figure 2. *MtNramp* gene family expression in roots and nodule. A, Gene expression in denodulated roots relative to the internal standard gene *Ubiquitin carboxyl-terminal hydrolase*. B, *MtNramp1* expression in nitrogen-fertilized roots (NFR), denodulated roots (DR), and nodules (Nod) relative to the internal standard gene *Ubiquitin carboxyl-terminal hydrolase*. C, Gene expression in the nodule relative to the internal standard gene *Ubiquitin carboxyl-terminal hydrolase*. Data are the mean ± SE of three independent experiments. n.d., No transcript was detected.

increased the iron uptake capability of the cells (Fig. 3B). Taken together, the results indicate that MtNramp1 is able to transport iron and manganese toward the cytosol.

MtNramp1 Is Localized in the Plasma Membrane of Zone II Cells

Nramp transporters are present in a wide range of organs and organelles (Thomine et al., 2000; Oomen et al., 2009; Yang et al., 2013). The precise location of the transporters is key to their biological roles, which range from metal uptake from soil (Cailliatte et al., 2010) to metal remobilization from intracellular reserves (Cailliatte et al., 2010; Lanquar et al., 2010). To determine whether *MtNramp1* expression is confined to roots and nodules, reverse transcription (RT)-PCR studies were carried out using RNA extracted from shoots, roots, and nodules from nodulated and non-nodulated *M. truncatula* plants. No *MtNramp1* transcript was detected in shoots regardless of symbiotic status (Fig. 4A).

To determine the tissue distribution of *MtNramp1* expression, *M. truncatula* seedlings were transformed with *Nramp1* promoter::*gus* fusions, where 2 kb of DNA immediately upstream of the *MtNramp1* start codon was selected as promoter. In symbiotic conditions, GUS activity was detected in nodulated roots and in the apical region of the nodule (Fig. 4B). Sections of these nodules showed that GUS expression was mostly confined to zone II (Fig. 4C), while it was detected in a perivascular layer in roots and also in a region that might be associated with the phloem (Fig. 4D).

The apical region of the nodule contains both zone I (meristem) and zone II (rhizobia infection and differentiation into bacteroids; Vasse et al., 1990). To verify the GUS-staining results and to determine MtNramp1 subcellular location, immunohistochemistry and confocal microscopy were used (Fig. 5). The complete MtNramp1 gene (exons plus introns) was cloned in frame with three hemagglutinin (3xHA) epitopes in its C-terminal end. To avoid misleading results due to overexpression, *MtNramp1* was cloned under the control of its own promoter, rather than the constitutive ubiquitin or 35S promoters. The lack of an adverse effect of the 3xHA epitope on protein transport capabilities was verified by complementation of the yeast *smf1* mutant with a plasmid constitutively expressing the *MtNramp1* coding sequence fused at the C terminus with the 3xHA tag (Supplemental Fig. S2). MtNramp1-HA was detected using a mouse anti-HA antibody and an Alexa594-conjugated anti-mouse secondary antibody (red). Its position within the nodule was mapped with the help of 4′,6-diamino-phenylindole (DAPI) to stain DNA (both eukaryotic and bacterial) and a constitutive GFP-expressing *Sinorhizobium meliloti* as inoculum (green).

As expected from the Nramp1 promoter-driven GUS activity, MtNramp-HA was localized to the apical region of the nodule and, more specifically, in the infection/differentiation zone (zone II), as indicated by the presence of GFP-expressing rhizobia and the abundance of infection threads (Fig. 5A). At higher magnification (Fig. 5B), MtNramp1-HA was found in cells where rhizobia were being released and in adjacent cell layers where rhizobia had increased in size following differentiation. MtNramp1-HA was located in the periphery of the cell, very likely in the plasma membrane. No colocalization with mature symbiosomes was observed (Fig. 5C). However, the tagged protein was also detected around the nucleus and in small

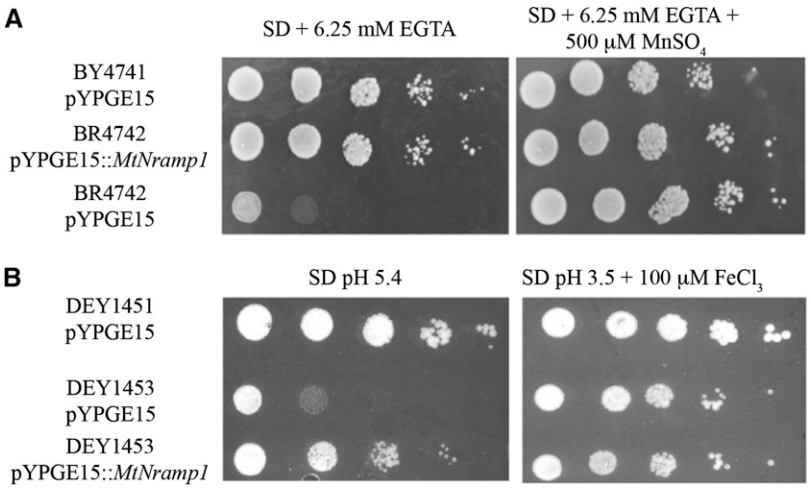

Figure 3. MtNramp1 transport assays. A, Manganese import. Yeast strain BY4741 was transformed with the pYPGE15 empty vector, while BY4741-derived BR4742 strain mutated in *smf1* was transformed either with empty pYPGE15 or with pYPGE15 containing *MtNramp1* coding DNA sequence (CDS). Serial dilutions (10×) of each transformant were grown for 3 d at 30°C on SD Glc medium with all the required amino acids. pH was buffered with 50 mM MES, and manganese levels were kept low with 6.25 mM EGTA. Manganese-replete positive controls were obtained by supplementing the plate with 500 μM $MnSO_4$. B, Iron import. Yeast strain DEY1451 was transformed with the pYPGE15 empty vector, while DEY1451-derived DEY1453 strain mutated in *fet3* and *fet4* was transformed either with empty pYPGE15 or with pYPGE15 containing *MtNramp1* CDS. Serial dilutions (10×) of each transformant were grown for 3 d at 30°C on SD Glc medium with all the required amino acids. Iron-replete positive controls were obtained by growing on pH 3.5 medium supplemented with 100 μM $FeCl_3$.

vesicles in the cytosol, probably the result of protein synthesis and sorting to the plasma membrane. No Alexa594 was detected in control plants transformed with untagged *MtNramp1* (Supplemental Fig. S3). To verify the plasma membrane localization, tobacco (*Nicotiana benthamiana*) leaves were transformed both with a construct expressing *MtNramp1* fused to GFP and plasmid encoding a plasma membrane-targeting motive fused to cyan fluorescent protein (CFP). GFP signal coincided with CFP fluorescent pattern (Fig. 5, D–F), indicating a plasma membrane localization of MtNramp1. Recent studies on gene expression in the different regions

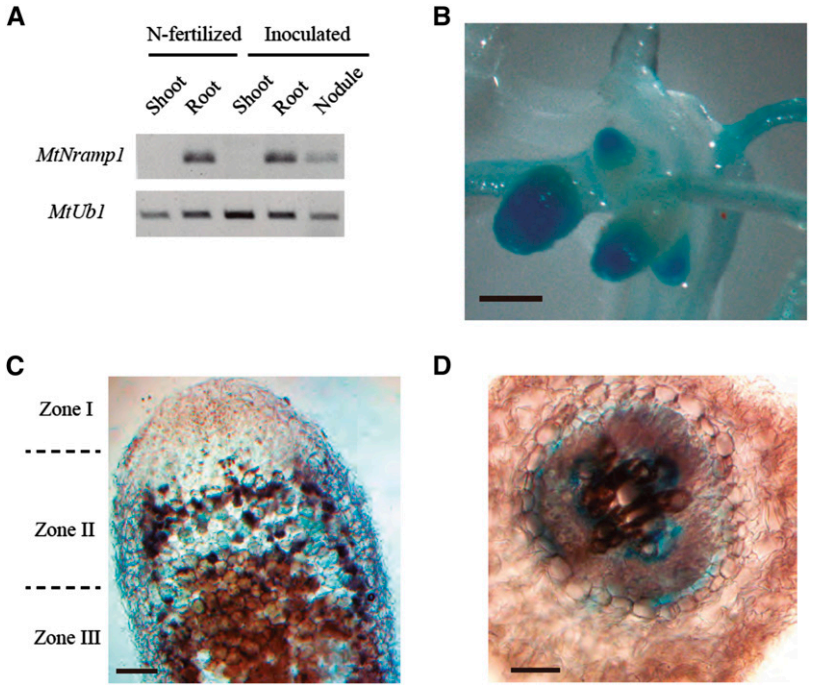

Figure 4. Organ and tissue location of *MtNramp1* transcripts. A, *MtNramp1* expression in shoots, roots, and nodules of unnodulated nitrogen-fertilized and nodulated plants. *MtUbiquitin carboxyl-terminal hydrolase1* (*MtUb1*) was used as positive control for RT-PCR. B, Histochemical staining of GUS activity in the root and nodules of *M. truncatula* plants transformed with plasmid pBI101 containing the *MtNramp1*-promoter::*gus* fusion. C, Longitudinal section of a GUS-stained nodule from *M. truncatula* plants transformed with plasmid pBI101 containing the *MtNramp1*-promoter::*gus* fusion. D, Cross section of a GUS-stained root from *M. truncatula* plants transformed with plasmid pBI101 containing the *MtNramp1*-promoter::*gus* fusion. Bars = 1 mm (B) and 0.1 mm (C and D).

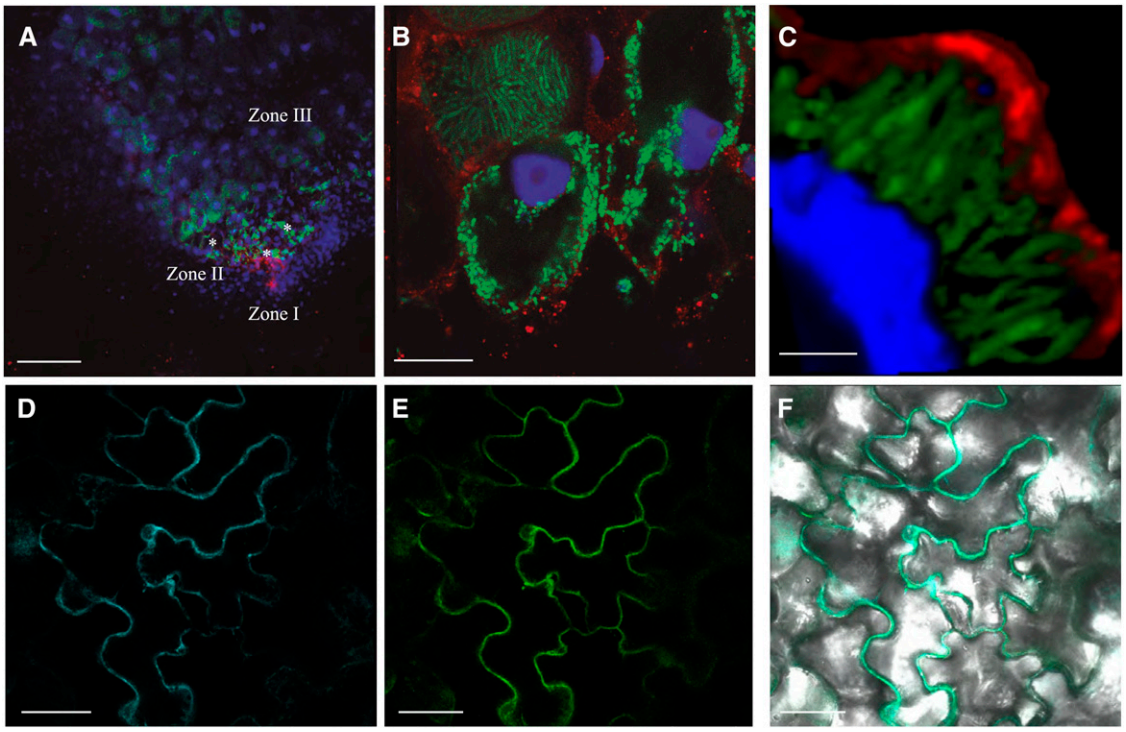

Figure 5. Subcellular localization of MtNramp1-HA. A, Cross section of a 28-dpi *M. truncatula* nodule infected with *S. meliloti* constitutively expressing GFP (green) and transformed with a vector expressing the fusion *MtNramp1-HA* under the regulation of its endogenous promoter. MtNramp1 localization was determined using an Alexa-594-conjugated antibody (red). DNA was stained with DAPI (blue). Infection threads are indicated with asterisks. B, Detailed view of rhizobia-infected cells in zone II. C, Three-dimensional reconstruction of a *MtNramp1-HA*-expressing cell. GFP-expressing *S. meliloti* cells are shown in green; red indicates the position of MtNramp1-HA, and blue is DAPI-stained DNA. D, Localization of plasma membrane marker pm-CFP transiently expressed in tobacco leaf cells. E, Localization of MtNramp1-GFP transiently expressed in the same cells. F, Overlay of pm-CFP and MtNramp1-GFP localization in tobacco leaf cells. Bars = 100 μm (A), 15 μm (B), 5 μm (C), and 50 μm (D–F).

of the nodule (Roux et al., 2014) and the public database derived from them (Symbimics) show that *MtNramp1* is expressed from zone I to zone III. Expression maxima of *MtNramp1* in late zone II and interzone II-III (Supplemental Fig. S4) are consistent with the pattern of distribution observed for MtNramp1-HA in the nodule. MtNramp1-HA was not detected in the vasculature of the nodules analyzed. However, in agreement with the GUS reporter assay, MtNramp1-HA was localized in a cell layer around the vasculature and, at very discrete points, associated with phloem/pericycle (Supplemental Materials and Methods S1; Supplemental Fig. S5, A–C). The perivascular cells corresponded with the endodermis, as Casparian strips were localized in the same layer as MtNramp1-HA (Supplemental Fig. S5, D and E).

Loss of *MtNramp1* Function Results in Reduced Nitrogenase Activity

To test the role of MtNramp1 in nitrogen fixation, *nramp1* mutants were isolated from a *Transposable Element from Nicotiana tabacum1* (*Tnt1*) insertion mutant collection (Tadege et al., 2008). Mutant line NF20333 had an insertion at position +744 within the fourth exon of the *MtNramp1* gene (Fig. 6A), which encodes the central part of the second transmembrane domain according to the structural model (Fig. 1B). Homozygous *nramp1-1* mutant plants had no detectable *Nramp1* transcript (Fig. 6B), indicating complete loss of function of this gene.

Given that *MtNramp1* was expressed in both nodulated and nonnodulated plants, the phenotype of the *nramp1-1* mutant was assessed under both conditions. Under nonsymbiotic conditions, *nramp1-1* mutants exhibited normal wild-type-like growth, fresh weight, and chlorophyll content regardless of iron levels in the nutrient solution (Supplemental Fig. S6). However, root iron content was significantly higher in the roots of *nramp1-1* than in the wild type when plants were grown with no additional iron in the nutrient solution (Supplemental Fig. S6D). The reverse was true for shoots, with iron levels lower in the mutant than in the wild type under these growth conditions (Supplemental Fig. S6D). Iron nutrition status was monitored using *M. truncatula Ferric Reduction Oxidase1* (*MtFRO1*; *Medtr8g028780*) expression, a marker of *M. truncatula* iron deficiency response (Andaluz et al., 2009).

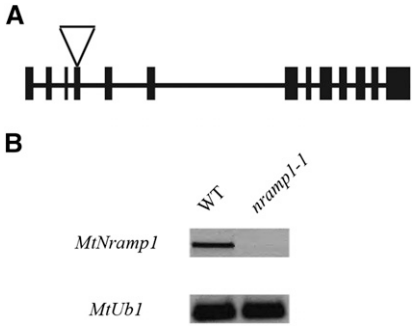

Figure 6. *MtNramp1 Tnt1* insertional knockout line. A, Position of the *Tnt1* insertion site for *nramp1-1* (NF20333). B, RT-PCR of *MtNramp1* expression in 28-dpi nodules in control (wild type [WT]) and *nramp1-1* *M. truncatula* lines. Expression of *MtUbiquitin carboxyl-terminal hydrolase* (*MtUb1*) was used as positive control.

Regardless of the iron levels in the nutritive solution, no significant differences were observed between *MtFRO1* expression in wild-type and *nramp1-1* lines (Supplemental Fig. S6E).

Under symbiotic conditions, without extra added nitrogen fertilizer, *nramp1-1* plants had severe growth defects (Fig. 7A). Mutant plants had mostly small white nodules, in contrast to the mostly larger, pink nodules of wild-type plants (Fig. 7B). Plant biomass was reduced by 79% in the mutant compared with the wild type (Fig. 7C). Nodulation was also impaired in the mutant, with 36% fewer nodules than the wild type (Fig. 7D). Nitrogenase activity of nodulated plants was measured using the acetylene reduction assay (Dilworth, 1966; Schöllhorn and Burris, 1966). Mutant plants grown under standard conditions showed a 40% reduction in nitrogenase activity compared with control transformed plants (Fig. 7E). These aberrant phenotypes of the *nramp1-1* mutant were not the result of insertions in other genes, as wild-type phenotypes were restored to *nramp1-1* roots transformed with wild-type *MtNramp1-HA* driven by its native promoter (the same construction used for the immunolocalization studies; Fig. 7, A–F). Furthermore, the phenotypes were associated with a reduction of iron uptake by the mutant, as wild-type phenotypes were restored when mutant plants were watered with an iron-fortified solution (Supplemental Fig. S7). *nramp1-1* had significantly higher iron levels in nodulated roots than in wild-type plants, while the reverse was true for nodules (Fig. 7F). Perl-DAB staining of wild-type and *nramp1-1* nodules showed neither changes in iron distribution nor the absence of major iron hotspots due to the mutation in *MtNramp1* (Supplemental Fig. S8, A and B). This result suggests that the difference in nodular iron content is merely due to the smaller nodule zone III developed by *nramp1-1* plants (less iron available means fewer ferroproteins and, therefore, a smaller nitrogen fixation zone). However, nodulated roots in *nramp1-1* showed some discrete iron hotspots in the apoplast not present in wild-type roots (Supplemental Fig. S8, C–E), corresponding to the increased iron concentration. No significant differences in iron content of shoots were found between mutant and wild-type plants under symbiotic conditions (Fig. 7F).

To determine whether reduced iron accumulation in mutant nodules resulted from loss of Nramp1 function in nodules, as opposed to roots, *nramp1-1* plants were transformed with *MtNramp1* driven by the nodule-specific promoter of the *Multidrug and Toxic Compound Extrusion* (*MATE*) gene, *Medtr6g081400*, which is also predominantly expressed in zone II (Fig. 8A; Supplemental Fig. S4). Targeted expression of *MtNramp1* to nodules of the *nramp1-1* mutant restored the normal growth to symbiotic *nramp1-1* plants (Fig. 8B). These plants also had active pink nodules instead of the small white nodules shown by *nramp1-1* plants (Fig. 8C), as well as an increase in the biomass (Fig. 8D) and in the total number of nodules (Fig. 8E) and an 85% increase in nitrogenase activity compared with the *nramp1-1* control (Fig. 8F).

Yeast complementation assays indicated that MtNramp1 was also a Mn^{2+} importer. To test whether MtNramp1 mutation had an effect on *M. truncatula* manganese homeostasis, *nramp1-1* symbiotic and nonsymbiotic phenotypes were assessed in plants watered either with the standard manganese concentrations or with a nutritive solution in which no manganese was added. No significant changes in the phenotype were observed in nonsymbiotic (Supplemental Fig. S9) or symbiotic conditions (Supplemental Fig. S10), other than a reduction in manganese content in *nramp1-1* roots under manganese-deficient conditions and an increase in *nramp1-1* shoots when watered with manganese-replete nutritive solution (Supplemental Figs. S9D and S10F).

DISCUSSION

Legumes are key to world agriculture (Graham and Vance, 2003). They are the main protein source in many areas of the world and, because of SNF, a viable alternative to the use of nitrogen fertilizers in agriculture (Smil, 1999). As in any plant, iron uptake and systemic distribution is critical in legumes. Like in other nongraminaceous plants, in legumes, iron uptake from soil follows what is known as Strategy I, i.e. Fe^{3+} solubility is increased by acidification of the surrounding soil and then Fe^{3+} is reduced by a ferroreductase to Fe^{2+}, which is imported into plants via specific transporters in the root epidermis (Andaluz et al., 2009). Once inside the plant, iron is used in legumes as in other plants, with one exception; in addition to the shoot, there is an extra iron sink during vegetative stages of growth, namely the root nodule (Tang et al., 1990).

Nodulation requires relatively large amounts of iron to synthesize the key enzymes involved in SNF (Brear et al., 2013; González-Guerrero et al., 2014). Synchrotron-based x-ray fluorescence results indicate that, at least in indeterminate nodules, iron is primarily

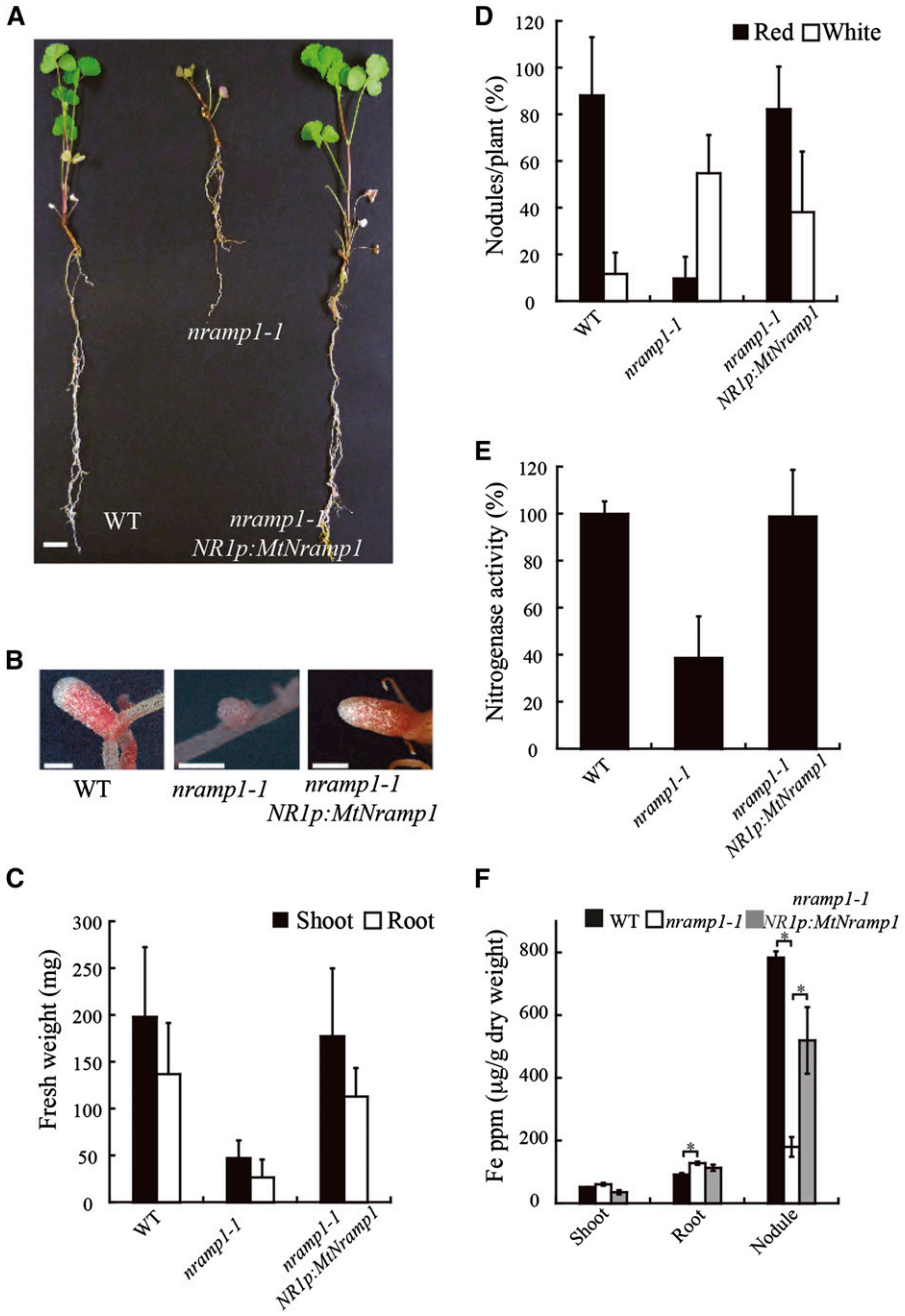

Figure 7. Symbiotic phenotype of *M. truncatula* wild type (WT), *nramp1-1*, and *nramp1-1* transformed with *MtNramp1* regulated under its endogenous promoter (*NR1p*). A, Growth of representative plants. Bar = 1 cm. B, Close view of representative nodules of each *M. truncatula* line. Bar = 1 mm. C, Fresh weight of shoots and roots. Data are the mean ± SE (n = 6–8 plants). D, Nodule number per plant; 100% = 5.67 nodules/plant. Data are the average ± SE (n = 7 plants). E, Nitrogenase activity in 28-dpi nodules. Acetylene reduction was measured in duplicate from two sets of five pooled plants. Data are the mean ± SE; 100% = 42.83 nmol ethylene h^{-1} g^{-1}. F, Iron content (μg g^{-1}) in 28-dpi plants. Bars indicate the average ± SE of two sets of five transformed plants. Asterisk indicates significant differences ($P \leq 0.05$).

delivered by the vasculature and released into the apoplast of zone II (Rodríguez-Haas et al., 2013). In this zone and probably in the interzone with the nitrogen-fixing zone III, iron has to be delivered from apoplast into cells before it is transported to the bacteria in symbiosomes. Our results indicate that MtNramp1 participates in iron translocation across the plasma membrane.

In contrast to soybean (Kaiser et al., 2003), *M. truncatula* does not encode a nodule-specific Nramp transporter. However, among the seven identified members of the *M. truncatula* Nramp family, *MtNramp1* showed by far the highest expression level in nodules. Yeast complementation assays indicated that MtNramp1 can transport iron and manganese into cells, consistent with a putative role in iron uptake by nodule cells infected with rhizobia. However, for this to be the case in *M. truncatula*, MtNramp1 should be localized in the plasma membrane in zone II cells.

Because iron is released into the apoplast of zone II cells, and because little or no iron remains in the zone III apoplast (Rodríguez-Haas et al., 2013), the conclusion is that Nramp or ZIP transporter(s) must mediate iron uptake from the apoplast into the cytosol of cells in this region of the nodule. Promoter::*gus* fusion data and the gene expression information from the

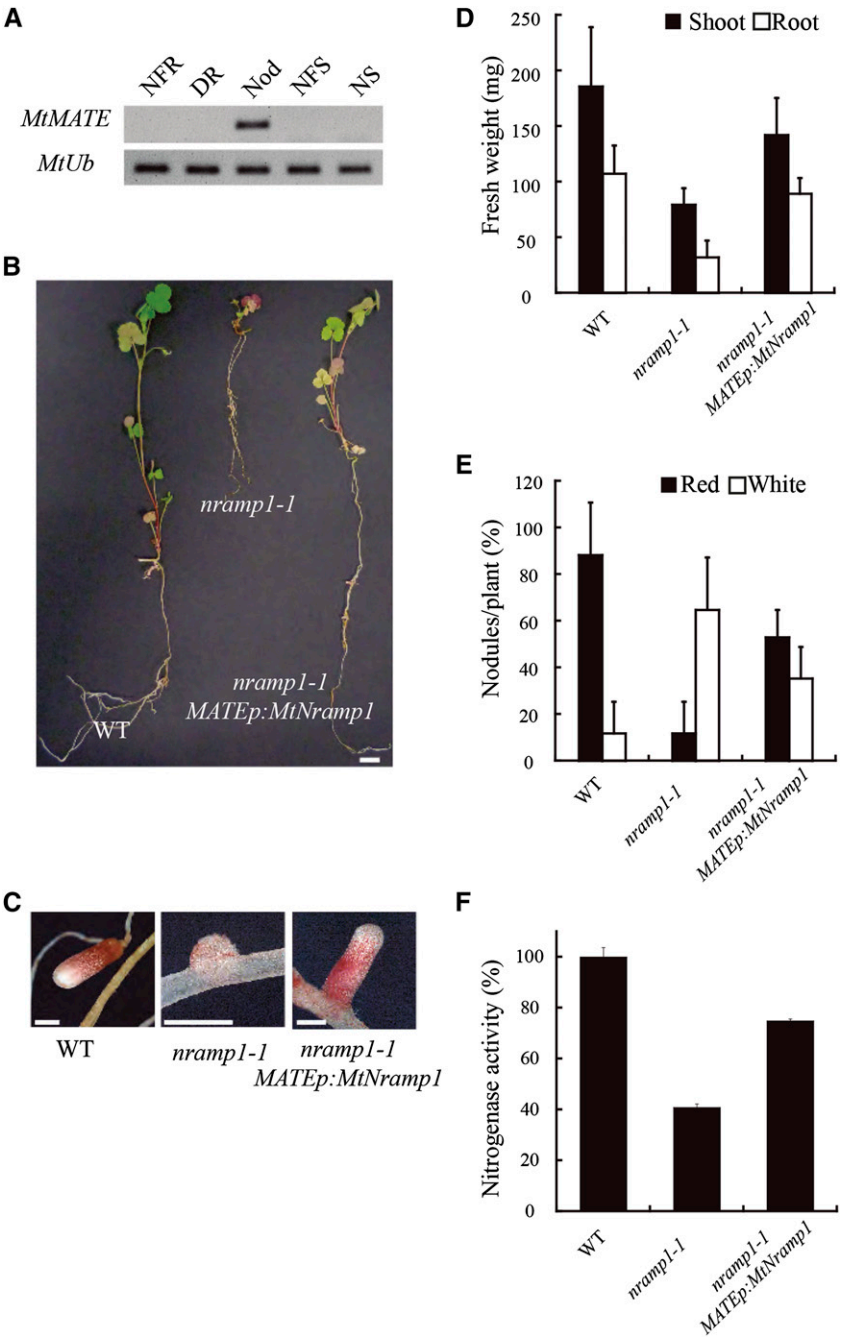

Figure 8. Complementation of *nramp1-1* phenotype by *MtNramp1* under the regulation of a nodule-specific promoter. A, Expression of *Medtr6g081400*, a nodule-specific MATE transporter used as a promoter source for the complementation construct. Expression of *MtUbiquitin carboxyl-terminal hydrolase* was used as positive control (*MtUb*). B, Growth of representative plants. C, Close view of representative nodules of each *M. truncatula* line. D, Fresh weight of shoots and roots. Data are the mean ± SE ($n = 4$ plants). E, Nodule number per plant; 100% = 4.25 nodules/plant. Data are the average ± SE ($n = 4$ plants). F, Nitrogenase activity in 28-dpi nodules. Acetylene reduction was measured in duplicate from two sets of five pooled plants. Data are the mean ± SE; 100% = 31.85 nmol ethylene h^{-1} g^{-1}. NFR, Nitrogen-fertilized roots; DR, denodulated roots; Nod, nodules; NFS, nitrogen-fertilized shoots; NS, shoots from nodulated plants; WT, wild type. Bars = 1 cm (B) and 1 mm (C).

Symbimics database for *MtNramp1* indicated that the gene is expressed in zone II of the nodule. Furthermore, immunolocalization studies of the transporter and its colocalization with plasma membrane markers indicated that it is located in the plasma membrane, in contrast to GmDMT1, which was found on the SM (Kaiser et al., 2003). This localization in *M. truncatula* does not appear to be an artifact of any of the fusions created, because (1) the addition of the HA tag did not have any major effect on the structure of the protein, as evidenced by the conservation of its transport capabilities in yeast and in *M. truncatula*, and (2) transcriptomic data on *MtNramp1* expression on different parts of the nodule (Roux et al., 2014) showed maximum expression in zone II and the interzone II-III, precisely where iron is most prevalent in the apoplast. These data may also explain why average *MtNramp1* transcript levels in whole nodules are lower than in roots; because MtNramp1 is confined to just a few cell layers, its mRNA is diluted by the mRNA from the many other nodule cells that do not express this gene.

Further evidence for a role of MtNramp1 in iron delivery for SNF is provided by the analysis of *nramp1-1* mutant plants. These plants accumulated higher levels of iron in roots than wild-type plants under low-iron growth conditions. This is consistent with the

localization of MtNramp1 in the root endodermis (the cell layer in which the Casparian strip was visualized). Mutation of a transporter involved in iron translocation into endodermal cells would result in iron accumulation in the root apoplast, and as a result, root iron content would be increased. This was observed in *nramp1-1* roots, where some iron deposits were detected in the apoplast. However, the role of MtNramp1 in nonsymbiotic conditions seems to be very limited, even under low-iron conditions, given that no additional phenotype was observed and that the iron deficiency response was not further induced in the mutant. Alternatively, other endodermal transporters might be masking a nonsymbiotic *nramp1-1* phenotype. Regardless of the mechanism, the fact that the *nramp1-1* mutant had neither significant difference in chlorophyll content compared with wild-type plants nor triggered the iron deficiency response indicates that sufficient iron was reaching the sink organs regardless of MtNramp1 activity. These results suggest that (1) MtNramp1 might be involved in the uptake of iron delivered to the endodermis through the apoplastic pathway, and (2) the

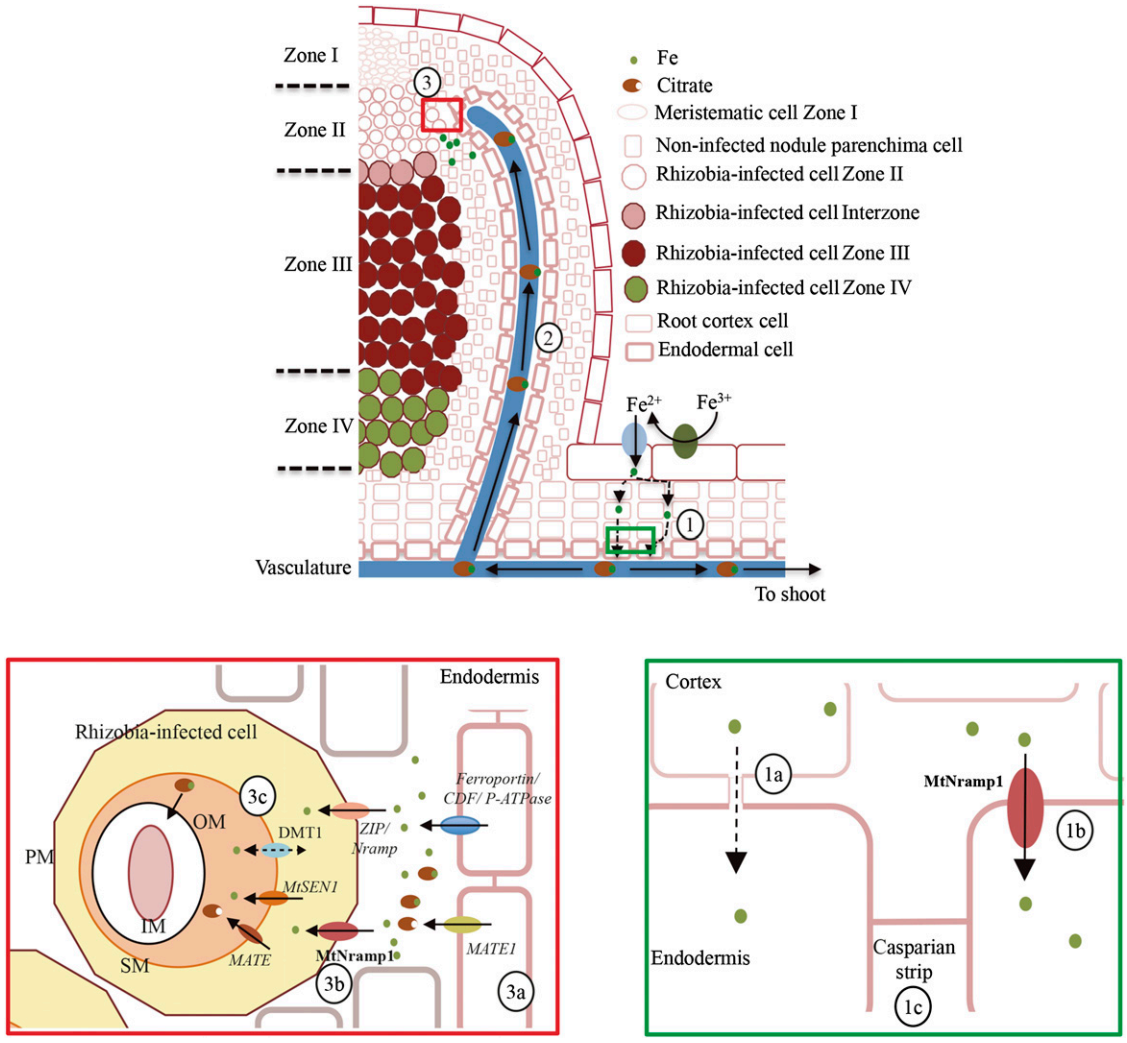

Figure 9. Proposed model of iron delivery to rhizobia-containing cells. Iron is incorporated from soil using Strategy 1 and delivered symplastically and apoplastically to the endodermal layer (1). Symplastic iron reaches the cytosol of endodermal cells (1a), while apoplastic iron is incorporated by these cells with the help of MtNramp1 (1b). This element is then transferred to the xylem (1c) to be transported to the rest of the plant as an iron-citrate complex (2). Iron is delivered to zone II of the nodule (3) and released from the vasculature in a process in which citrate efflux is likely to be necessary. A MATE family member homologous to LjMATE1 might facilitate citrate efflux (3a). MtNramp1 translocates iron across the plasma membrane (3b). In this role, an additional metal transporter (ZIP or YSL) could also be involved. Once in the cytosol, iron is likely to be transported across the SM by MtSEN1 in a process that might be assisted by another MATE family transporter (3c). An *M. truncatula* GmDMT1 ortholog could also participate in iron transport either by introducing iron or rather by effluxing iron to prevent overload of the peribacteroidal space. Putative transporters predicted to play a role in metal transport in the nodule are indicated in italics. PM, Plasma membrane; SM, symbiosome membrane; IM, inner membrane; OM, outer membrane; CDF, cation diffusion facilitator.

iron that reaches the endodermis through the symplastic pathway is sufficient to fulfill the plant iron requirements in nonsymbiotic conditions.

In stark contrast to nonsymbiotic plants, *nramp1-1* plants grown under symbiotic conditions, without substantial mineral nitrogen, had severe growth defects, with a dramatic reduction of biomass. This was accompanied by a reduction of nodulation and nitrogenase activity in these plants. All these phenotypes were suppressed by adding high levels of iron-Sequestrene chelate to the nutrient solution or by expressing the wild-type *MtNramp1* in the mutant plants, indicating the importance of MtNramp1 in iron delivery for SNF. However, it might be argued that this defect was due to iron not being introduced in the vasculature and, consequently, not being transported to the nodule, in view of the reduced iron content in *nramp1-1* nodules (Fig. 7F). To test this hypothesis, *MtNramp1* was fused to a promoter from a nodule-specific *MATE* gene with a similar expression pattern to *MtNramp1* in nodules. This chimera was able to improve the growth of *nramp1-1* as well as increase the number of functional nodules, as indicated by the more abundant red nodules and their increased nitrogenase activity. Therefore, although some of the *nramp1-1* phenotype is due to iron being retained in the root, a substantial part is likely due to an inability of nodule cells to take up iron from the apoplast.

While playing a role in iron homeostasis, MtNramp1 does not seem to have any significant role on manganese nutrition, despite its ability to transport Mn^{2+} shown in yeast (possibly an acquired ability that could result from overexpressing the transporter in a heterologous system). The observed reduction of manganese content in *nramp1-1* roots under some conditions indicated that MtNramp1 is not involved in manganese transport in planta. The changes in manganese levels by *MtNramp1* mutation could be the result of the plant adapting to an altered long-distance iron transport, a consequence to the changes in iron distribution caused by *MtNramp1* mutation.

In conclusion, MtNramp1 appears to play a major role in iron uptake from the apoplast into rhizobia-containing cells in zone II of the nodule and a minor role in root-to-shoot iron translocation. This is in contrast to another Nramp transporter, GmDMT1 of soybean, which has been localized in the symbiosome (Kaiser et al., 2003). Other transporters might assist MtNramp1 in transporting iron in nodules, as the *nramp1-1* mutant produced some partially functional nodules. MtNramp7 could potentially play this role, because it is the only other *M. truncatula* Nramp family member with a pattern of expression similar

Table I. *Primers used in this study*

Name	Sequence	Use
5MtNramp1-*Xba*I	AATCTAGAATGGCACATCAAGAAGTGAAT	Cloning of *MtNramp1* cDNA in pYGPE15
3MtNramp1-*Bam*HI	TTGGATCCTCACAACCTAGGTCCCTCTG	Cloning of *MtNramp1* cDNA in pYGPE15
5MtNramp1p-*Hin*dIII	GGAAGCTTTTTTTATTTGAACTTAGAATTA	Cloning of *MtNramp1* promoter in pBI101
3MtNramp1p-*Bam*HI	TTGGATCCGTTTACTATTACTATTCACTC	Cloning of *MtNramp1* promoter in pBI101
5GWMtNramp1p	GGGGACAAGTTTGTACAAAAAAGCAGGCTATTGAACT-TAGAATTAAACCAC	Cloning of *MtNramp1* promoter and coding sequence in Gateway vectors
3GWMtNramp1	GGGGACCACTTTGTACAAGAAAGCTGGGTACAACCTA-GGTCCCTCTGGTCG	Cloning of *MtNramp1* promoter and coding sequence in Gateway vectors/C-terminal GFP fusion
5MtUBqF	GAACTTGTTGCATGGGTCTTGA	Quantitative reverse transcription (q)PCR of *MtUbiquitin carboxyl-terminal hydrolase*
3MtUBqR	CATTAAGTTTGACAAAGAGAAAGAGACAGA	qPCR of *MtUbiquitin carboxyl-terminal hydrolase*
5MtNramp1 + 1GW	GGGGACAAGTTTGTACAAAAAAGCAGGCTTCATGGCA-CATCAAGAAGTGAAT	C-terminal GFP fusion of MtNramp1
5MtNRAMP1-1533	AAGGGGTTTGTAAACGATGGTCAGT	qPCR of *MtNramp1*
3MtNRAMP1-1659	GCTCTCTAAAATGACTTGAAAGCAA	qPCR of *MtNramp1*
5MtNRAMP2-1500	AACCAAGTGGAAAAAGGAATTGTGG	qPCR of *MtNramp2*
3MtNRAMP2-1617	TTGGATCCTTTATTCTGGTAGTGGT	qPCR of *MtNramp2*
5MtNRAMP3-1431	TTTTCAGGCATGGCAGTATATTTGG	qPCR of *MtNramp3*
3MtNRAMP3-1598	TGGACTACTTCTCTGAGGCAATTGC	qPCR of *MtNramp3*
5MtNRAMP4-1427	CTTCCTTTCTGAGGTGAACAGCGTA	qPCR of *MtNramp4*
3MtNRAMP4-1586	TCCATATTTTTAATGTTGTGTAACTTGTGT	qPCR of *MtNramp4*
5MtNRAMP5-1387	TTTCCTCTGAAGTGAGTGGAGCAGT	qPCR of *MtNramp5*
3MtNRAMP5-1565	AACTTTGCGTGGTAGCTACTATTTG	qPCR of *MtNramp5*
5MtNRAMP6-1527	TGTGCAACAGCATGGATTTCATTTA	qPCR of *MtNramp6*
3MtNRAMP6-1663	CTATATATTCACATCATCATCACCAAAAA	qPCR of *MtNramp6*
5MtNRAMP7-1423	AATAACCGCTGCATATGTTGCATTC	qPCR of *MtNramp7*
3MtNRAMP7-1549	CTGCAGTTCTAAGGATCCATTATTCA	qPCR of *MtNramp7*
5MtFRO1qF	GGTGACACGTGGATCATCTG	qPCR of *MtFRO1*
3MtFRO1qR	TTGCAATCCACAGGAACAAA	qPCR of *MtFRO1*

to that of *MtNramp1*. However, *MtNramp7* exhibited low expression levels in the nodule, and according to the database Symbimics, it is expressed mostly in zone III instead of zone II. Therefore, it cannot be ruled out that a ZIP or even a Yellow Stripe-Like (YSL) transporter may contribute to iron uptake into nitrogen-fixing cells. Taking into account these considerations, a tentative model of iron transport to indeterminate nodules is presented in Figure 9. In this model, iron is incorporated from soil using Strategy I and guided to the vasculature via symplastic and apoplastic routes. To reach the vessels, apoplastic iron has to be taken up by endodermal cells, very likely with the assistance of MtNramp1. Iron is released from the vasculature in zone II of the nodule by a yet-to-be-identified transporter. Citrate may play a role in this release, because mutation of the MATE transporter *LjMATE1* in *L. japonicus* results in iron accumulation in the nodule vasculature (Takanashi et al., 2013). Although this observation was made in determinate-type nodules, iron released from the vasculature is likely to follow a similar mechanism in indeterminate nodules. Iron accumulates in the apoplast, where MtNramp1 and perhaps other transporters move it into the cytosol. From there, a putative homolog of LjSEN1 may be responsible for iron translocation across the SM (Hakoyama et al., 2012). In this process, an additional citrate transporter might play a role, given that iron-citrate is the preferred source of chelated iron for some rhizobia (LeVier et al., 1996). Future studies will be directed toward testing this model as well as toward determining the identity of transporters responsible for iron release from the vasculature.

MATERIALS AND METHODS

Biological Materials and Growth Conditions

Medicago truncatula R108 seeds were scarified by incubating for 7 min with concentrated H_2SO_4. Washed, scarified seeds were surface sterilized with 50% (v/v) bleach for 90 s and left overnight in sterile water. After 48 h at 4°C, seeds were germinated in water-agar plates at 22°C for 48 h. Seedlings were transferred to sterilized perlite pots and inoculated with *Sinorhizobium meliloti* 2011 or *S. meliloti* 2011 transformed with pHC60 (Cheng and Walker, 1998), as indicated. Plants were grown in a greenhouse with 16 h of light and 22°C and watered every 2 d with Jenner's solution or water, alternatively (Brito et al., 1994). When indicated, water was supplemented with 0.5 g L^{-1} Sequestrene (Syngenta). Nodules were collected 28 dpi. Nonnodulated plants were similarly grown, but instead of being inoculated with *S. meliloti*, they were watered every 2 weeks with solutions supplemented with 2 mM NH_4NO_3. For hairy-root transformations, *M. truncatula* seedlings were transformed with *Agrobacterium rhizogenes* ARqua1 carrying the appropriate binary vector as described (Boisson-Dernier et al., 2001). Tobacco (*Nicotiana benthamiana*) agroinfiltration experiments were carried out by transforming leaves with the plasmid constructs in *Agrobacterium tumefaciens* C58C1 (Deblaere et al., 1985). Tobacco plants were grown in the greenhouse under the same conditions as *M. truncatula*.

For heterologous expression, the yeast (*Saccharomyces cerevisiae*) strains DEY1453 (*ade2/+ can1/can1 his3/his3 leu2/leu2 trp1/trp1 ura3/ura3 fet3-2::HIS3/fet3-2::HIS3 fet4-1::LEU2/fet4-1::LEU2*), DEY1451 (*MATa/MATa ade2/+ can1/can1 his3/his3 leu2/leu2 trp1/trp1 ura3/ura3*; Dix et al., 1994), BY4741 (*his3 leu2 met1 ura3*), and BR4742 (*his3 leu2 met1 ura3 Δsmf1*; Thermo Scientific) were used. DEY1453 needs 100 μM iron supplementation and pH 3.5 to grow (Dix et al., 1994), and BY1457 cannot grow when 6.25 mM manganese-chelating EGTA is added to the medium unless supplemented with manganese (Portnoy et al., 2000). All strains were grown in synthetic dextrose (SD) or yeast peptone dextrose (Sherman et al., 1986) medium supplemented with necessary auxotrophic requirements with 2% (w/v) Glc as the carbon source.

RNA Extraction and qPCR

RNA was obtained using Tri-Reagent (Life Technologies), DNase treated and cleaned with RNeasy Mini Kit (Qiagen). Putative DNA contamination was checked by PCR on RNA extraction using *M. truncatula Ubiquitin carboxyl-terminal hydrolase* (*Medtr4g077320.1*) primers (Table I). RNA quality was verified on a denaturing agarose gel. cDNA was obtained from 1 μg of DNA-free RNA using SuperScript III reverse transcriptase (Invitrogen).

Gene expression was studied by quantitative real-time RT-PCR (9700, Applied Biosystems) with primers indicated in Table I and standardized to the *M. truncatula Ubiquitin carboxyl-terminal hydrolase* gene. Real-time cycler conditions have been previously described (González-Guerrero et al., 2010). Determinations were carried out with RNA extracted from three independent biological samples, with the threshold cycle determined in triplicate. The relative levels of transcription were calculated using the $2^{-\Delta Ct}$ method. In all RT-PCR reactions, a non-RT control was used to detect any possible DNA contamination.

Yeast Complementation Assays

MtNramp1 cDNA was cloned between the *Xba*I and *Bam*HI sites of yeast expression vector pYPGE15. Restriction sites were added to *MtNramp1* CDS by PCR-using primers 5MtNramp1-*Xba*I and 3MtNramp1-*Bam*HI (Table I). Yeast transformations were performed using a lithium acetate-based method (Schiestl and Gietz, 1989). Cells transformed with pYPGE15 or pYPGE15::*MtNramp1* were selected in SD medium by uracil autotrophy. For phenotypic tests, DEY1453 and DEY1451 were plated in SD, pH 3.5, supplemented with 100 μM $FeCl_3$, and in SD, pH 5.4. BY4741 and BR4742 transformants were plated in SD plates supplemented with 50 mM MES, pH 6.0, and 6.25 mM EGTA, with or without 500 μM $MnSO_4$.

GUS Staining

pMtNramp1::gus was constructed by amplifying 2 kb upstream of the *MtNramp1* start codon using primers 5MtNramp1p-*Hin*dIII and 3MtNramp1p-*Bam*HI (Table I). The digested product was ligated into the *Bam*HI/*Hin*dIII sites in pBI101 (Jefferson et al., 1987). Hairy-root transformation was performed as described above. GUS activity was measured in roots of 28-dpi plants as described (Vernoud et al., 1999).

Confocal Microscopy Detection of MtNramp1-HA

A DNA fragment containing the full-length *MtNramp1* genomic region and the 2 kb upstream of its start codon was cloned in pGWB13 (Nakagawa et al., 2007) using Gateway Technology (Invitrogen). This vector adds three C-terminal HA tags in frame. Hairy-root transformation was performed as described above. Transformed plants were inoculated with *S. meliloti* 2011 containing the pHC60 plasmid that constitutively expresses GFP. Nodules from 28-dpi plants were fixed in 4% (w/v) paraformaldehyde and 2.5% (w/v) Suc in phosphate-buffered saline (PBS) at 4°C overnight. Nodules were then washed in PBS, and 100-μm sections were obtained with a Vibratome 1000 Plus. Sections were then dehydrated in a methanol series (30%, 50%, 70%, and 100% [v/v] in PBS) for 5 min and then rehydrated. Cell walls were permeabilized with 2% (w/v) cellulose in PBS for 1 h at room temperature and treated with 0.1% (v/v) Tween 20 for 15 min. Sections were blocked with 5% (w/v) bovine serum albumin in PBS and incubated with an anti-HA mouse monoclonal antibody (Sigma) for 2 h at room temperature. After washing the primary antibody, an Alexa594-conjugated anti-mouse rabbit monoclonal antibody (Sigma) was added to the sections for 1 h at room temperature. After washing away the unbound antibody, DNA was stained with DAPI. Images were acquired with a confocal laser-scanning microscope (Leica SP8).

Transient *MtNramp1* Expression by Agroinfiltration in Tobacco Leaves

Experiments were performed as described by Voinnet et al. (2003). MtNramp1 CDS was fused to GFP at the C terminus by cloning in pGWB5

(Nakagawa et al., 2007) using Gateway Technology (Invitrogen). These constructs and the plasma membrane marker pm-CFP pBIN (Nelson et al., 2007) were introduced into *A. tumefaciens* C58C1 (Deblaere et al., 1985) by electroporation. Transformed cells were selected on Luria-Bertani plates supplemented with Rifampicin (50 μg mL^{-1}) and Kanamycin (50 μg mL^{-1}). The transformants were grown in liquid Luria-Bertani medium to late exponential phase. Cells were then centrifuged and resuspended to an optical density at 600 nm of 1 in 10 mM MES, pH 5.6, containing 10 mM $MgCl_2$ and 150 μM acetosyringone. These cells were mixed with an equal volume of *A. tumefaciens* C58C1 expressing the silencing suppressor p19 of *Tomato bushy stunt virus* (pCH32 35S:p19; Voinnet et al., 2003). Bacterial suspensions were incubated for 3 h at room temperature and then injected into young leaves of 4-week-old tobacco plants. Leaves were examined after 3 d by confocal laser-scanning microscopy.

Isolation of a *Tnt1* Mutant for *MtNramp1*

Insertional mutant for *MtNramp1* was identified in the course of reverse genetic screening performed on retrotransposon *Tnt1* mutant population (Tadege et al., 2008). The procedure was based on nested PCR as described previously (Cheng et al., 2011).

Acetylene Reduction Assay

Nitrogenase activity was measured by the acetylene reduction assay (Hardy et al., 1968). Nitrogen fixation was assayed in mutant and control plants 28 dpi in 25-mL tubes fitted with rubber stoppers. Each tube contained five independently transformed plants. Two and one-half milliliters of air inside was replaced with 2.5 mL of acetylene. Tubes were incubated at room temperature for 30 min. Gas samples (0.5 mL) were analyzed in a Shimadzu GC-8A gas chromatograph fitted with a Porapak N column. The amount of ethylene produced was determined by measuring the height of the ethylene peak relative to background. Each point consists of two tubes, each with five pooled plants. After measurements, nodules were recovered from roots to measure their weight.

Metal Content Determination

Total reflection x-ray fluorescence analysis was used to determine iron content in 28-dpi mutant nodules isolated and pooled from 10 different plants. Analyses were carried out at Total Reflection X-Ray Fluorescence Laboratory (Interdepartmental Research Service, Universidad Autónoma de Madrid). Inductively coupled plasma optical emission spectrometry was carried out at the Unit of Metal Analysis (Scientific and Technology Centres, Universidad de Barcelona).

Bioinformatics

To identify *M. truncatula* Nramp family members, BLASTN and BLASTX searches were carried out in the *M. truncatula* Genome Project site (http://www.jcvi.org/medicago/index.php). Sequences from model *Nramp* genes were obtained from the Transporter Classification Database (http://www.tcdb.org/; Saier et al., 2014). Protein sequence comparison and unrooted tree visualization were carried out using ClustalW (http://www.ebi.ac.uk/Tools/msa/clustalw2/) and FigTree (http://tree.bio.ed.ac.uk/software/figtree/). Structural modeling was done using SWISS-MODEL (http://swissmodel.expasy.org/; Guex et al., 2009).

Statistical Tests

Data were analyzed by Student's unpaired *t* test to calculate statistical significance of observed differences. Test results with *P* values less than 0.05 were considered as statistically significant.

Supplemental Data

The following supplemental materials are available.

Supplemental Figure S1. *MtNramp* gene family expression.

Supplemental Figure S2. MtNramp1-HA yeast complementation assay.

Supplemental Figure S3. Antibody-specific control for immunolocalization.

Supplemental Figure S4. Expression in the different *M. truncatula* nodule zones.

Supplemental Figure S5. MtNramp1-HA localization in the root.

Supplemental Figure S6. Phenotype of *nramp1-1* under nonsymbiotic conditions.

Supplemental Figure S7. Iron complementation of the *nramp1-1* phenotype.

Supplemental Figure S8. Iron distribution in roots and nodules of wild-type and *nramp1-1* plants.

Supplemental Figure S9. Nonsymbiotic phenotype of *nramp1-1* under Mn deficiency conditions.

Supplemental Figure S10. Symbiotic phenotype of *nramp1-1* under two different Mn concentrations.

Supplemental Materials and Methods S1. Perl-DAB and Casparian strip staining methods.

ACKNOWLEDGMENTS

We thank Dr. Alonso Rodríguez-Navarro (Universidad Politécnica de Madrid) for providing plasmid pYPGE15, Dr. David Eide (University of Wisconsin, Madison) for the strain *fet3/fet4* and its parental strain, Dr. Benoit Lefebvre (Laboratoire des Interactions Plantes Microorganismes) for the pBI101 vector, Dr. Florian Frugier (Institut des Sciences du Vegétal) for the pFRN vector, Dr. Rosario Haro (Universidad Politécnica de Madrid) for the organelle-specific markers, Dr. Regla Bustos (Instituto Nacional de Investigaciones Agroalimentarias) for the agroinfiltration protocol, Dr. Larry Peterson for the Casparian strip visualization method, and Dr. Tsuyoshi Nakagawa (Shiimane University) for the pGWB vectors.

Received December 3, 2014; accepted March 25, 2015; published March 27, 2015.

LITERATURE CITED

Andaluz S, Rodríguez-Celma J, Abadía A, Abadía J, López-Millán AF (2009) Time course induction of several key enzymes in *Medicago truncatula* roots in response to Fe deficiency. Plant Physiol Biochem **47:** 1082–1088

Appleby CA (1984) Leghemoglobin and *Rhizobium* respiration. Annu Rev Plant Physiol **35:** 443–478

Askwith C, Eide D, Van Ho A, Bernard PS, Li L, Davis-Kaplan S, Sipe DM, Kaplan J (1994) The *FET3* gene of *S. cerevisiae* encodes a multicopper oxidase required for ferrous iron uptake. Cell **76:** 403–410

Belouchi A, Kwan T, Gros P (1997) Cloning and characterization of the OsNramp family from *Oryza sativa*, a new family of membrane proteins possibly implicated in the transport of metal ions. Plant Mol Biol **33:** 1085–1092

Boisson-Dernier A, Chabaud M, Garcia F, Bécard G, Rosenberg C, Barker DG (2001) *Agrobacterium rhizogenes*-transformed roots of *Medicago truncatula* for the study of nitrogen-fixing and endomycorrhizal symbiotic associations. Mol Plant Microbe Interact **14:** 695–700

Brear EM, Day DA, Smith PM (2013) Iron: an essential micronutrient for the legume-rhizobium symbiosis. Front Plant Sci **4:** 359

Brewin NJ (1991) Development of the legume root nodule. Annu Rev Cell Biol **7:** 191–226

Brito B, Palacios JM, Hidalgo E, Imperial J, Ruiz-Argüeso T (1994) Nickel availability to pea (*Pisum sativum* L.) plants limits hydrogenase activity of *Rhizobium leguminosarum* bv. *viciae* bacteroids by affecting the processing of the hydrogenase structural subunits. J Bacteriol **176:** 5297–5303

Cailliatte R, Lapeyre B, Briat JF, Mari S, Curie C (2009) The NRAMP6 metal transporter contributes to cadmium toxicity. Biochem J **422:** 217–228

Cailliatte R, Schikora A, Briat JF, Mari S, Curie C (2010) High-affinity manganese uptake by the metal transporter NRAMP1 is essential for *Arabidopsis* growth in low manganese conditions. Plant Cell **22:** 904–917

Cheng HP, Walker GC (1998) Succinoglycan is required for initiation and elongation of infection threads during nodulation of alfalfa by *Rhizobium meliloti*. J Bacteriol **180:** 5183–5191

Cheng X, Wen J, Tadege M, Ratet P, Mysore KS (2011) Reverse genetics in *Medicago truncatula* using *Tnt1* insertion mutants. Methods Mol Biol **678:** 179–190

Curie C, Alonso JM, Le Jean M, Ecker JR, Briat JF (2000) Involvement of NRAMP1 from *Arabidopsis thaliana* in iron transport. Biochem J **347:** 749–755

Deblaere R, Bytebier B, De Greve H, Deboeck F, Schell J, Van Montagu M, Leemans J (1985) Efficient octopine Ti plasmid-derived vectors for *Agrobacterium*-mediated gene transfer to plants. Nucleic Acids Res **13:** 4777–4788

Dilworth MJ (1966) Acetylene reduction by nitrogen-fixing preparations from *Clostridium pasteurianum*. Biochim Biophys Acta **127:** 285–294

Dix DR, Bridgham JT, Broderius MA, Byersdorfer CA, Eide DJ (1994) The *FET4* gene encodes the low affinity Fe(II) transport protein of *Saccharomyces cerevisiae*. J Biol Chem **269:** 26092–26099

Downie JA (2014) Legume nodulation. Curr Biol **24:** R184–R190

Ehrnstorfer IA, Geertsma ER, Pardon E, Steyaert J, Dutzler R (2014) Crystal structure of a SLC11 (NRAMP) transporter reveals the basis for transition-metal ion transport. Nat Struct Mol Biol **21:** 990–996

Forbes JR, Gros P (2001) Divalent-metal transport by NRAMP proteins at the interface of host-pathogen interactions. Trends Microbiol **9:** 397–403

González-Guerrero M, Matthiadis A, Sáez AN, Long TA (2014) Fixating on metals: new insights into the role of metals in nodulation and symbiotic nitrogen fixation. Front Plant Sci **5:** 45

González-Guerrero M, Raimunda D, Cheng X, Argüello JM (2010) Distinct functional roles of homologous Cu^+ efflux ATPases in *Pseudomonas aeruginosa*. Mol Microbiol **78:** 1246–1258

Graham PH, Vance CP (2003) Legumes: importance and constraints to greater use. Plant Physiol **131:** 872–877

Grotz N, Guerinot ML (2006) Molecular aspects of Cu, Fe and Zn homeostasis in plants. Biochim Biophys Acta **1763:** 595–608

Guex N, Peitsch MC, Schwede T (2009) Automated comparative protein structure modeling with SWISS-MODEL and Swiss-PdbViewer: a historical perspective. Electrophoresis (Suppl 1) **30:** S162–S173

Hakoyama T, Niimi K, Yamamoto T, Isobe S, Sato S, Nakamura Y, Tabata S, Kumagai H, Umehara Y, Brossuleit K, et al (2012) The integral membrane protein SEN1 is required for symbiotic nitrogen fixation in *Lotus japonicus* nodules. Plant Cell Physiol **53:** 225–236

Hardy RW, Holsten RD, Jackson EK, Burns RC (1968) The acetylene-ethylene assay for N_2 fixation: laboratory and field evaluation. Plant Physiol **43:** 1185–1207

Jefferson RA, Kavanagh TA, Bevan MW (1987) GUS fusions: β-glucuronidase as a sensitive and versatile gene fusion marker in higher plants. EMBO J **6:** 3901–3907

Kaiser BN, Moreau S, Castelli J, Thomson R, Lambert A, Bogliolo S, Puppo A, Day DA (2003) The soybean NRAMP homologue, GmDMT1, is a symbiotic divalent metal transporter capable of ferrous iron transport. Plant J **35:** 295–304

Kondorosi E, Banfalvi Z, Kondorosi A (1984) Physical and genetic analysis of a symbiotic region of *Rhizobium meliloti*: identification of nodulation genes. Mol Gen Genet **193:** 445–452

Lanquar V, Lelièvre F, Bolte S, Hamès C, Alcon C, Neumann D, Vansuyt G, Curie C, Schröder A, Krämer U, et al (2005) Mobilization of vacuolar iron by AtNRAMP3 and AtNRAMP4 is essential for seed germination on low iron. EMBO J **24:** 4041–4051

Lanquar V, Ramos MS, Lelièvre F, Barbier-Brygoo H, Krieger-Liszkay A, Krämer U, Thomine S (2010) Export of vacuolar manganese by AtNRAMP3 and AtNRAMP4 is required for optimal photosynthesis and growth under manganese deficiency. Plant Physiol **152:** 1986–1999

LeVier K, Day DA, Guerinot ML (1996) Iron uptake by symbisomes from soybean root nodules. Plant Physiol **111:** 893–900

Mayer JE, Pfeiffer WH, Beyer P (2008) Biofortified crops to alleviate micronutrient malnutrition. Curr Opin Plant Biol **11:** 166–170

Miller RW, Yu Z, Zarkadas CG (1993) The nitrogenase proteins of *Rhizobium meliloti*: purification and properties of the MoFe and Fe components. Biochim Biophys Acta **1163:** 31–41

Mizuno T, Usui K, Horie K, Nosaka S, Mizuno N, Obata H (2005) Cloning of three ZIP/Nramp transporter genes from a Ni hyperaccumulator plant *Thlaspi japonicum* and their Ni^{2+}-transport abilities. Plant Physiol Biochem **43:** 793–801

Nakagawa T, Kurose T, Hino T, Tanaka K, Kawamukai M, Niwa Y, Toyooka K, Matsuoka K, Jinbo T, Kimura T (2007) Development of series of gateway binary vectors, pGWBs, for realizing efficient construction of fusion genes for plant transformation. J Biosci Bioeng **104:** 34–41

Nelson BK, Cai X, Nebenführ A (2007) A multicolored set of in vivo organelle markers for co-localization studies in Arabidopsis and other plants. Plant J **51:** 1126–1136

Nevo Y, Nelson N (2006) The NRAMP family of metal-ion transporters. Biochim Biophys Acta **1763:** 609–620

Oldroyd GE (2013) Speak, friend, and enter: signalling systems that promote beneficial symbiotic associations in plants. Nat Rev Microbiol **11:** 252–263

Oomen RJFJ, Wu J, Lelièvre F, Blanchet S, Richaud P, Barbier-Brygoo H, Aarts MGM, Thomine S (2009) Functional characterization of NRAMP3 and NRAMP4 from the metal hyperaccumulator *Thlaspi caerulescens*. New Phytol **181:** 637–650

Ott T, van Dongen JT, Günther C, Krusell L, Desbrosses G, Vigeolas H, Bock V, Czechowski T, Geigenberger P, Udvardi MK (2005) Symbiotic leghemoglobins are crucial for nitrogen fixation in legume root nodules but not for general plant growth and development. Curr Biol **15:** 531–535

Portnoy ME, Liu XF, Culotta VC (2000) *Saccharomyces cerevisiae* expresses three functionally distinct homologues of the nramp family of metal transporters. Mol Cell Biol **20:** 7893–7902

Preisig O, Zufferey R, Thöny-Meyer L, Appleby CA, Hennecke H (1996) A high-affinity cbb3-type cytochrome oxidase terminates the symbiosis-specific respiratory chain of *Bradyrhizobium japonicum*. J Bacteriol **178:** 1532–1538

Rodríguez-Haas B, Finney L, Vogt S, González-Melendi P, Imperial J, González-Guerrero M (2013) Iron distribution through the developmental stages of *Medicago truncatula* nodules. Metallomics **5:** 1247–1253

Rosakis A, Köster W (2005) Divalent metal transport in the green microalga *Chlamydomonas reinhardtii* is mediated by a protein similar to prokaryotic Nramp homologues. Biometals **18:** 107–120

Roth LE, Stacey G (1989) Bacterium release into host cells of nitrogen-fixing soybean nodules: the symbiosome membrane comes from three sources. Eur J Cell Biol **49:** 13–23

Roux B, Rodde N, Jardinaud MF, Timmers T, Sauviac L, Cottret L, Carrère S, Sallet E, Courcelle E, Moreau S, et al (2014) An integrated analysis of plant and bacterial gene expression in symbiotic root nodules using laser-capture microdissection coupled to RNA sequencing. Plant J **77:** 817–837

Rubio MC, Becana M, Sato S, James EK, Tabata S, Spaink HP (2007) Characterization of genomic clones and expression analysis of the three types of superoxide dismutases during nodule development in *Lotus japonicus*. Mol Plant Microbe Interact **20:** 262–275

Ruiz-Argüeso T, Emerich DW, Evans HJ (1979) Hydrogenase system in legume nodules: a mechanism of providing nitrogenase with energy and protection from oxygen damage. Biochem Biophys Res Commun **86:** 259–264

Saier MH Jr, Reddy VS, Tamang DG, Västermark A (2014) The transporter classification database. Nucleic Acids Res **42:** D251–D258

Schiestl RH, Gietz RD (1989) High efficiency transformation of intact yeast cells using single stranded nucleic acids as a carrier. Curr Genet **16:** 339–346

Schöllhorn R, Burris RH (1966) Study of intermediates in nitrogen fixation. Fed Proc **25:** 710

Segond D, Dellagi A, Lanquar V, Rigault M, Patrit O, Thomine S, Expert D (2009) NRAMP genes function in *Arabidopsis thaliana* resistance to *Erwinia chrysanthemi* infection. Plant J **58:** 195–207

Sherman F, Fink GR, Hicks JB (1986) Methods in Yeast Genetics. Cold Spring Harbor Lab Press, Plainview, NY

Smil V (1999) Nitrogen in crop production: an account of global flows. Global Biogeochem Cycles **13:** 647–662

Sprent JI (2007) Evolving ideas of legume evolution and diversity: a taxonomic perspective on the occurrence of nodulation. New Phytol **174:** 11–25

Supek F, Supekova L, Nelson H, Nelson N (1996) A yeast manganese transporter related to the macrophage protein involved in conferring resistance to mycobacteria. Proc Natl Acad Sci USA **93:** 5105–5110

Tadege M, Wen J, He J, Tu H, Kwak Y, Eschstruth A, Cayrel A, Endre G, Zhao PX, Chabaud M, et al (2008) Large-scale insertional mutagenesis using the *Tnt1* retrotransposon in the model legume *Medicago truncatula*. Plant J **54:** 335–347

Takanashi K, Yokosho K, Saeki K, Sugiyama A, Sato S, Tabata S, Ma JF, Yazaki K (2013) LjMATE1: a citrate transporter responsible for iron supply to the nodule infection zone of *Lotus japonicus*. Plant Cell Physiol **54:** 585–594

Tang C, Robson AD, Dilworth MJ (1990) The role of iron in nodulation and nitrogen fixation in *Lupinus angustifolius* L. New Phytol **114:** 173–182

Tang CX, Robson AD, Dilworth MJ, Kuo J (1992) Microscopic evidence on how iron-deficiency limits nodule initiation in *Lupinus angustifolius* l. New Phytol **121:** 457–467

Terry RE, Soerensen KU, Jolley VD, Brown JC (1991) The role of active *Bradyrhizobium japonicum* in iron stress response of soy-beans. Plant Soil **130:** 225–230

Thomine S, Wang R, Ward JM, Crawford NM, Schroeder JI (2000) Cadmium and iron transport by members of a plant metal transporter family in Arabidopsis with homology to Nramp genes. Proc Natl Acad Sci USA **97:** 4991–4996

Timmers ACJ, Soupène E, Auriac MC, de Billy F, Vasse J, Boistard P, Truchet G (2000) Saprophytic intracellular rhizobia in alfalfa nodules. Mol Plant Microbe Interact **13:** 1204–1213

Udvardi M, Poole PS (2013) Transport and metabolism in legume-rhizobia symbioses. Annu Rev Plant Biol **64:** 781–805

van Rhijn P, Vanderleyden J (1995) The *Rhizobium*-plant symbiosis. Microbiol Rev **59:** 124–142

Vasse J, de Billy F, Camut S, Truchet G (1990) Correlation between ultrastructural differentiation of bacteroids and nitrogen fixation in alfalfa nodules. J Bacteriol **172:** 4295–4306

Vernoud V, Journet EP, Barker DG (1999) *MtENOD20*, a Nod factor-inducible molecular marker for root cortical cell activation. Mol Plant Microbe Interact **12:** 604–614

Vert G, Grotz N, Dédaldéchamp F, Gaymard F, Guerinot ML, Briat JF, Curie C (2002) IRT1, an *Arabidopsis* transporter essential for iron uptake from the soil and for plant growth. Plant Cell **14:** 1223–1233

Voinnet O, Rivas S, Mestre P, Baulcombe D (2003) An enhanced transient expression system in plants based on suppression of gene silencing by the p19 protein of tomato bushy stunt virus. Plant J **33:** 949–956

Yamaji N, Sasaki A, Xia JX, Yokosho K, Ma JF (2013) A node-based switch for preferential distribution of manganese in rice. Nat Commun **4:** 2442

Yang M, Zhang W, Dong H, Zhang Y, Lv K, Wang D, Lian X (2013) OsNRAMP3 is a vascular bundles-specific manganese transporter that is responsible for manganese distribution in rice. PLoS ONE **8:** e83990

SUPPLEMENTAL MATERIAL AND METHODS

Casparian strip visualization.

After immunolocalization of MtNramp1-HA in roots and subsequent analysis by confocal microscopy, these sections were stained using the berberine-aniline blue method (Brundrett et al., 1988). Briefly, sections were incubated with 0.1% berberine hemi-sulphate (Sigma) in water for 1 h. After washing with water, samples were incubated in 0.5% aniline blue in water for 30 min and then rinsed with water. Finally, sections were transferred to 0.1% $FeCl_3$ in 50% glycerol for several minutes and mounted in the same solution. Images were obtained using a confocal laser-scanning microscope (Leica SP8, Wetzlar, Germany).

Iron distibution visualization

Roots and nodules from 28 dpi wild type and *nramp1-1* plants were collected and fixed in 0.25% glutaraldehyde, 4% formaldehyde, 2.5% sucrose in 50 mM potassium phosphate buffer (pH 7.4) at 4 ºC overnight. Sample were then dehydratated using ethanol series and embedded in LR-White resin (London Resin Company Ltd, UK) (Rodríguez-Haas et al., 2013). Finally, nodules were placed in gelatine capsules, filled with resin and polymerized at 60ºC for 24 h. Serial thin sections (1µm) were cut with a Reichert Ultracut S ultramicrotome (Leica, Vienna, Austria) fitted with a diamond knife. Sections for nodule structure analysis were stained with a mixture of 1% (w/v) toluidine blue in aqueous 1% sodium borate and 1% (w/v) methylene blue in water. Iron distribution was visualized using the Perl-DAB method (Roschzttardtz et al., 2009). Direct observation of sections was performed under a Zeiss Axiophot photomicroscope (Carl Zeiss, Oberkochen, Germany) with an attached digital camera (Leica DFC 420C, Heerburgg, Switzerland). A minimum of three nodules and roots per treatment and three sections per sample were examined.

Brundrett M, Enstone D, Peterson C (1988) A berberine-aniline blue fluorescent staining procedure for suberin, lignin, and callose in plant tissue. Protoplasma **146:** 133-142

Rodríguez-Haas B, Finney L, Vogt S, González-Melendi P, Imperial J, González-Guerrero M (2013) Iron distribution through the developmental stages of *Medicago truncatula* nodules. Metallomics **5:** 1247-1253

Roschzttardtz H, Conejero G, Curie C, Mari S (2009) Identification of the endodermal vacuole as the iron storage compartment in the Arabidopsis embryo. Plant Physiol **151:** 1329-1338

SUPPLEMENTAL FIGURE LEGENDS

Supplemental Figure S1. *MtNramp* gene family expression. Gene expression of the corresponding *MtNramp* gene in nitrogen-fertilized roots (NFR), denodulated roots (DR) and nodules (Nod) relative to the internal standard gene *ubiquitin carboxyl-terminal hydrolase*. Data are the mean ± SE of three independent experiments.

Supplemental Figure S2. *MtNramp1-HA* yeast complementation assay. Yeast strain BY4741 was transformed with the pYPGE15 empty vector, while BY4741-derived BR4742 strain mutated in *smf1* was transformed with either pYPGE15 alone, or with pYPEG15 containing *MtNramp1* CDS, or with pYPGE15 harbouring *MtNramp1* CDS with a C-terminal 3xHA tag. Serial dilutions (10x) of each transformant were grown for 3 days at 30ºC on SD Glucose media with all the required amino acids. pH was buffered with 50 mM MES and Mn levels were kept low with 6.25 mM EGTA. Mn-replete positive controls were obtained by supplementing the plate with 500 µM $MnSO_4$.

Supplemental Figure S3. Antibody-specificity control for immunolocalization. Cross section of a 28 dpi *M. truncatula* nodule infected with *S. meliloti* constitutively expressing GFP (green) and transformed with a vector expressing *MtNramp1* under the regulation of its endogenous promoter. MtNramp1 localization was determined using an Alexa 594-conjugated antibody (red). DNA was stained with DAPI (blue). Infection threads are indicated with asterisks. Scale bar represents 100 µm.

Supplemental Figure S4. Expression in the different *M. truncatula* nodule zones. (A) *MtNramp1***.** (B) Nodule-specific MATE transporter *Medtr6g081400*. ZI indicates zone I; ZIId, distal zone II (region closest to zone I); ZIIp, proximal zone II; IZ is the interzone between zone II and zone III; and ZIII, zone III. Data were obtained from the Symbimics database (https://iant.toulouse.inra.fr/symbimics).

Supplemental Figure S5. MtNramp1-HA localization in the root. (A) Confocal microscopy localization of MtNramp1-HA in a cross section of a 28 dpi *M. truncatula* root transformed with a vector expressing *MtNramp1* under the regulation of its endogenous promoter. MtNramp1 position was determined using an Alexa 594-

conjugated antibody (red). DNA and xylem was stained with DAPI (blue). (B) Bright-field image of the cross section. (C) Overlay of panels A and B. (D) Close-up of overlaid MtNramp1-HA localization in *M. truncatula* transformed roots (detected with an Alexa 594-conjugated antibody in red) and bright-field image. (E) Casparian strip localization (blue) detected with the berberine-aniline blue method. (F) Overlay of panels D and E. Scale bars represent 50 µm (panels A-C) or 10 µm (panels D-F).

Supplemental Figure S6. Phenotype of *nramp1-1* under non-symbiotic conditions. (A) Growth of representative plants. Scale bar represents 1 cm. Fe concentrations in nutritive solutions used are indicated below. (B) Fresh weight of shoots and roots. Data are the mean ± SE (n = 5 plants). (C) Chlorophyll content. Data are the mean ± SE (n = 3 plants). (D) Iron content in roots and shoots of wild-type and *nramp1-1* plants under two different iron fertilization levels. Data are the mean ± SE of two sets of five pooled plants. * indicates significative differences ($p \leq 0.05$). (F) *MtFRO1* expression in wild type and nramp1-1 plants under two different iron fertilization levels. Data are the mean ± SE of three independet experiments. * indicates significative differences ($p \leq 0.05$).

Supplemental Figure S7. **Iron complementation of *nramp1-1* phenotype.** (A) Growth of representative plants. Scale bar represents 1 cm. (B) Fresh weight of shoots and roots. Data are the mean ± SE (n = 8 plants). (C) Nodule number per plant. 100 % = 4.25 nodules/plant. Data are the average ± SE (n=8-10 plants). (D) Nitrogenase activity in 28 dpi nodules. Acetylene reduction was measured in duplicate from two sets of five pooled plants. Data are the mean ± SE. 100% = 61.17 nmol ethylene $h^{-1}g^{-1}$.

Supplemental Figure S8. Iron distribution in roots and nodules of wild type and *nramp1-1* plants. (A) wild type *M. truncatula* nodule and (B) *nramp1-1 M. truncatula* nodule. Left panels show reference sections stained with toluidine blue and methylene blue, the boxed regions represent the approximate area corresponding to the Perl-DAB-stained (right panel) which shows the iron distribution. Nodule zones are indicated. (C) Iron distribution in wild type *M. truncatula* root. Left panel shows a root section stained with toluidine blue and methylene blue, the boxed region represents the approximate area corresponding to the Perl-DAB-stained right panel. (D) Iron distribution in *nramp1-1 M. truncatula* root. Left panel shows a reference section stained with toluidine blue and methylene blue, the boxed region represents the approximate área

corresponding to the Perl-DAB-stained right panel. Arrowheads indicate regions of iron accumulation. (E) Close-up view of Perl-DAB stained *nramp1-1* root (corresponding to the boxed area of the right panel in D). Arrowheads indicate regions of iron accumulation. Scale bars represent 100 μm (A-C, and left panel D), 50 μm (right panel D), or 10 μm (E).

Supplemental Figure S9. Non-symbiotic phenotype *nramp1-1* under Mn deficiency conditions. (A) Growth of representative plants. Scale bar represents 1 cm. Manganese concentrations in nutritive solutions used are indicated below. (B) Fresh weight of shoots and roots. Data are the mean ± SE (n = 5 plants). (C) Chlorophyll content. Data are the mean ± SE (n = 3 plants). (D) Manganese content in roots and shoots of wild-type and nramp1-1 plants under two different manganese fertilization levels. Data are the mean ± SE of two sets of five pooled plants. * indicates significative differences ($p \leq 0.05$).

Supplemental Figure S10. Symbiotic phenotype of *nramp1-1* under two different Mn concentrations (A) Growth of representative plants. Scale bar represents 1 cm. (B) Close view of representative nodules of each M. truncatula line. Scale bar represents 1 mm. (C) Fresh weight of shoots and roots. Data are the mean ± SE (n = 6-8 plants). (D) Nodule number per plant. 100 % = 4.21 nodules/plant. Data are the average ± SE (n= 7 plants). (E) Nitrogenase activity in 28 dpi nodules. Acetylene reduction was measured in duplicate from two sets of five pooled plants. Data are the mean ± SE. 100% = 26.69 nmol ethylene h-1g-1. (F) Mn content (ppm) in 28 dpi plants. Bars indicate the average ± SE of two sets of 5 transformed plants. * indicates significant differences ($p \leq 0.05$).

SUPPLEMENTAL FIGURE S1

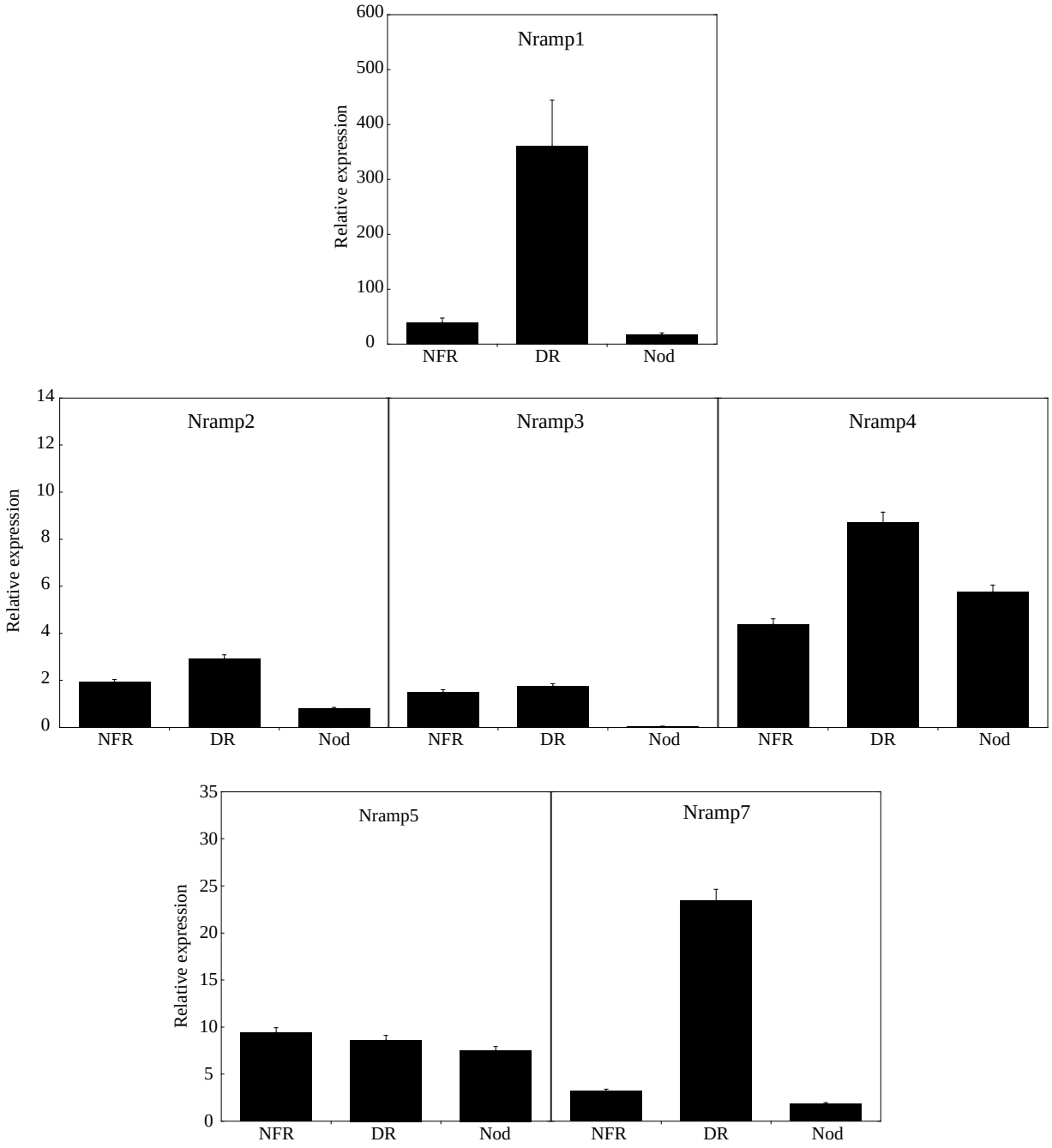

Supplemental Figure S1. *MtNramp* gene family expression. Gene expression of the corresponding *MtNramp* gene in nitrogen-fertilized roots (NFR), denodulated roots (DR) and nodules (Nod) relative to the internal standard gene *ubiquitin carboxyl-terminal hydrolase*. Data are the mean ± SE of three independent experiments.

SUPPLEMENTAL FIGURE S2

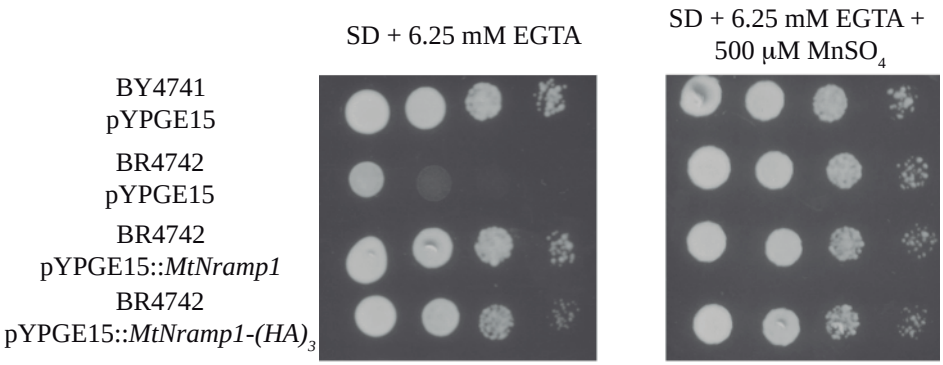

Supplemental Figure S2. *MtNramp1-HA* yeast complementation assay. Yeast strain BY4741 was transformed with the pYPGE15 empty vector, while BY4741-derived BR4742 strain mutated in *smf1* was transformed with either pYPGE15 alone, or with pYPEG15 containing *MtNramp1* CDS, or with pYPGE15 harbouring *MtNramp1* CDS with a C-terminal 3xHA tag. Serial dilutions (10x) of each transformant were grown for 3 days at 30ºC on SD Glucose media with all the required amino acids. pH was buffered with 50 mM MES and Mn levels were kept low with 6.25 mM EGTA. Mn-replete positive controls were obtained by supplementing the plate with 500 µM $MnSO_4$.

SUPPLEMENTAL FIGURE S3

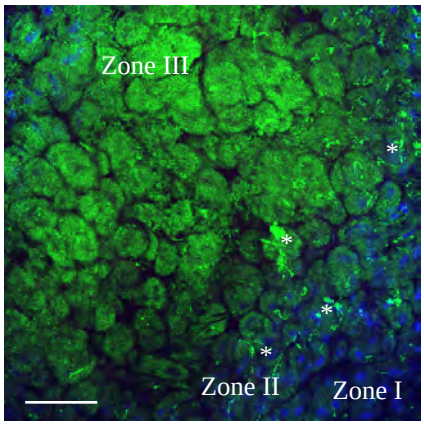

Supplemental Figure S3. Antibody-specificity control for immunolocalization. Cross section of a 28 dpi *M. truncatula* nodule infected with *S. meliloti* constitutively expressing GFP (green) and transformed with a vector expressing *MtNramp1* under the regulation of its endogenous promoter. MtNramp1 localization was determined using an Alexa 594-conjugated antibody (red). DNA was stained with DAPI (blue). Infection threads are indicated with asterisks. Scale bar represents 100 μm.

SUPPLEMENTAL FIGURE S4

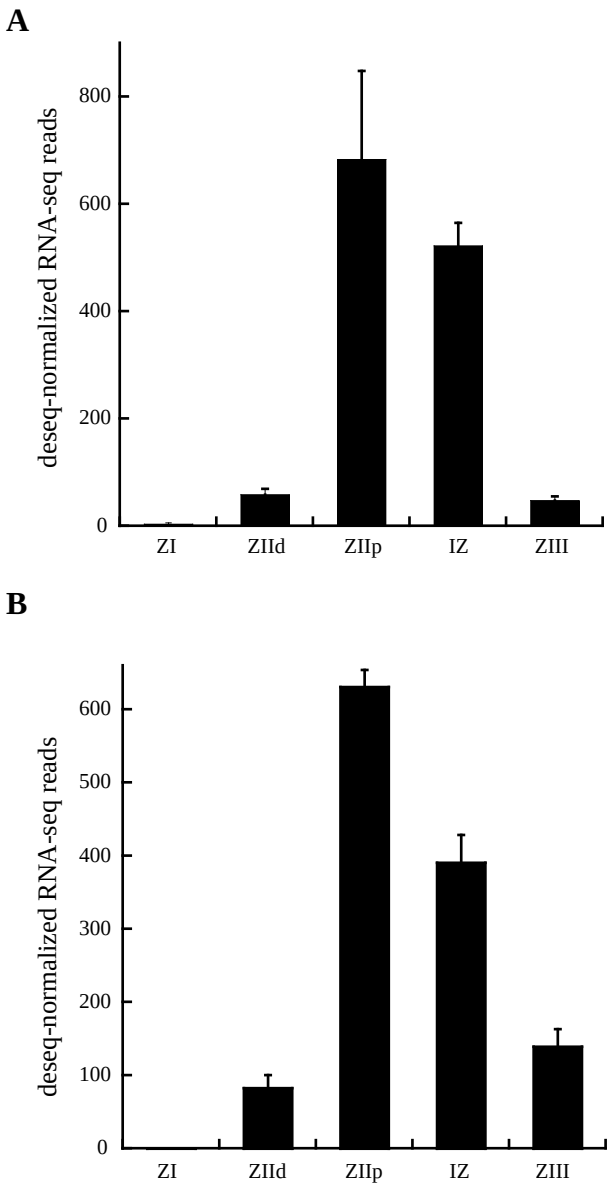

Supplemental Figure S4. Expression in the different *M. truncatula* nodule zones. (A) MtNramp1. (B) Nodule-specific MATE transporter *Medtr6g081400*. ZI indicates zone I; ZIId, distal zone II (region closest to zone I); ZIIp, proximal zone II; IZ is the interzone between zone II and zone III; and ZIII, zone III. Data were obtained from the Symbimics database (https://iant.toulouse.inra.fr/symbimics).

SUPPLEMENTAL FIGURE S5

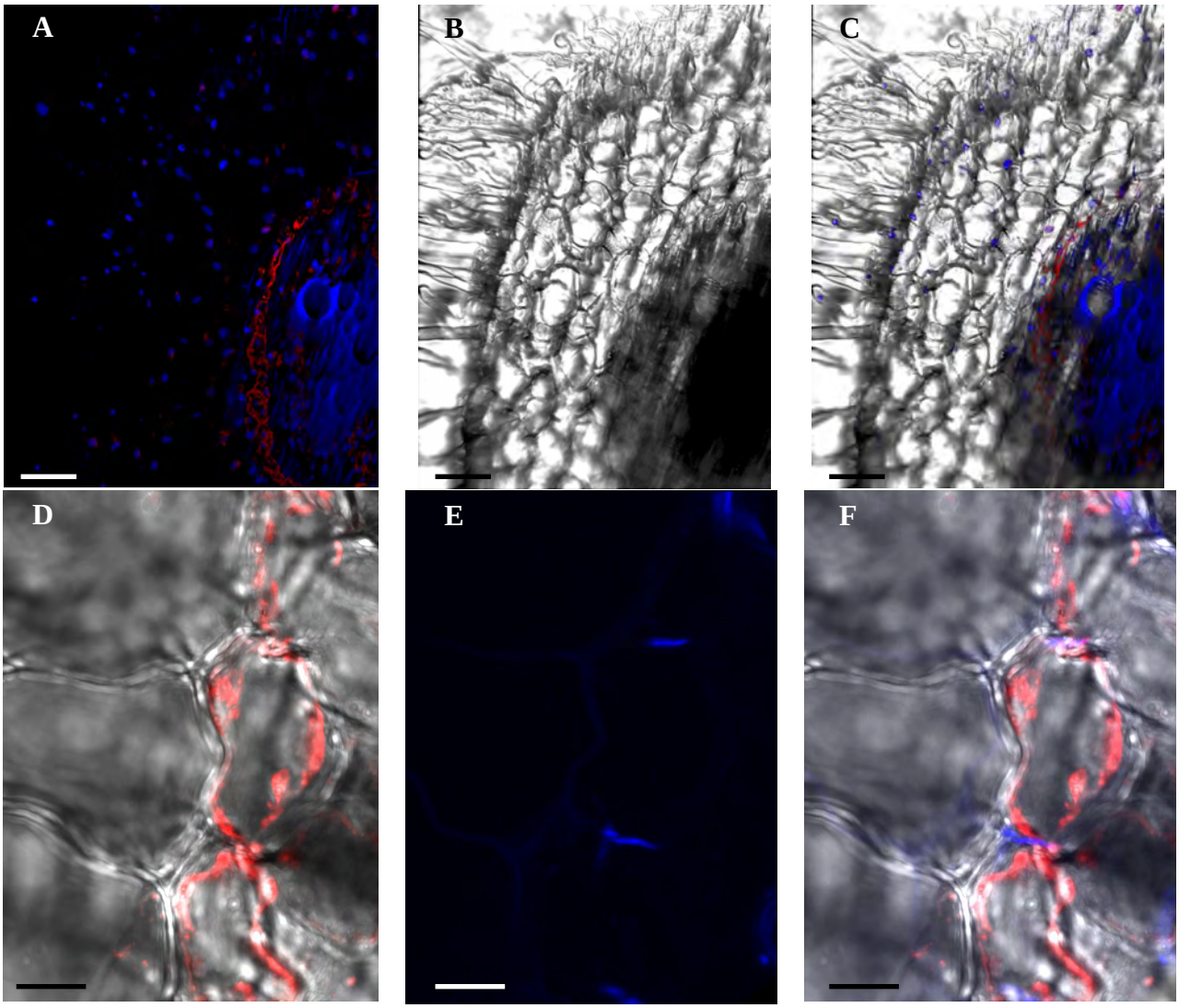

Supplemental Figure S5. MtNramp1-HA localization in the root. (A) Confocal microscopy localization of MtNramp1-HA in a cross section of a 28 dpi *M. truncatul*a root transformed with a vector expressing *MtNramp1* under the regulation of its endogenous promoter. MtNramp1 position was determined using an Alexa 594-conjugated antibody (red). DNA and xylem was stained with DAPI (blue). (B) Optical image of the cross section. (C) Overlay of panels A and B. (D) Close-up of overlaid MtNramp1-HA localization in *M. truncatula* transformed roots (detected with an Alexa 594-conjugated antibody in red) and optical image. (E) Casparian strip localization (blue) detected with the berberine-aniline blue method. (F) Overlay of panels D and E. Scale bars represent 50 μm (panels A-C) or 10 μm (panels D-F).

SUPPLEMENTAL FIGURE S6

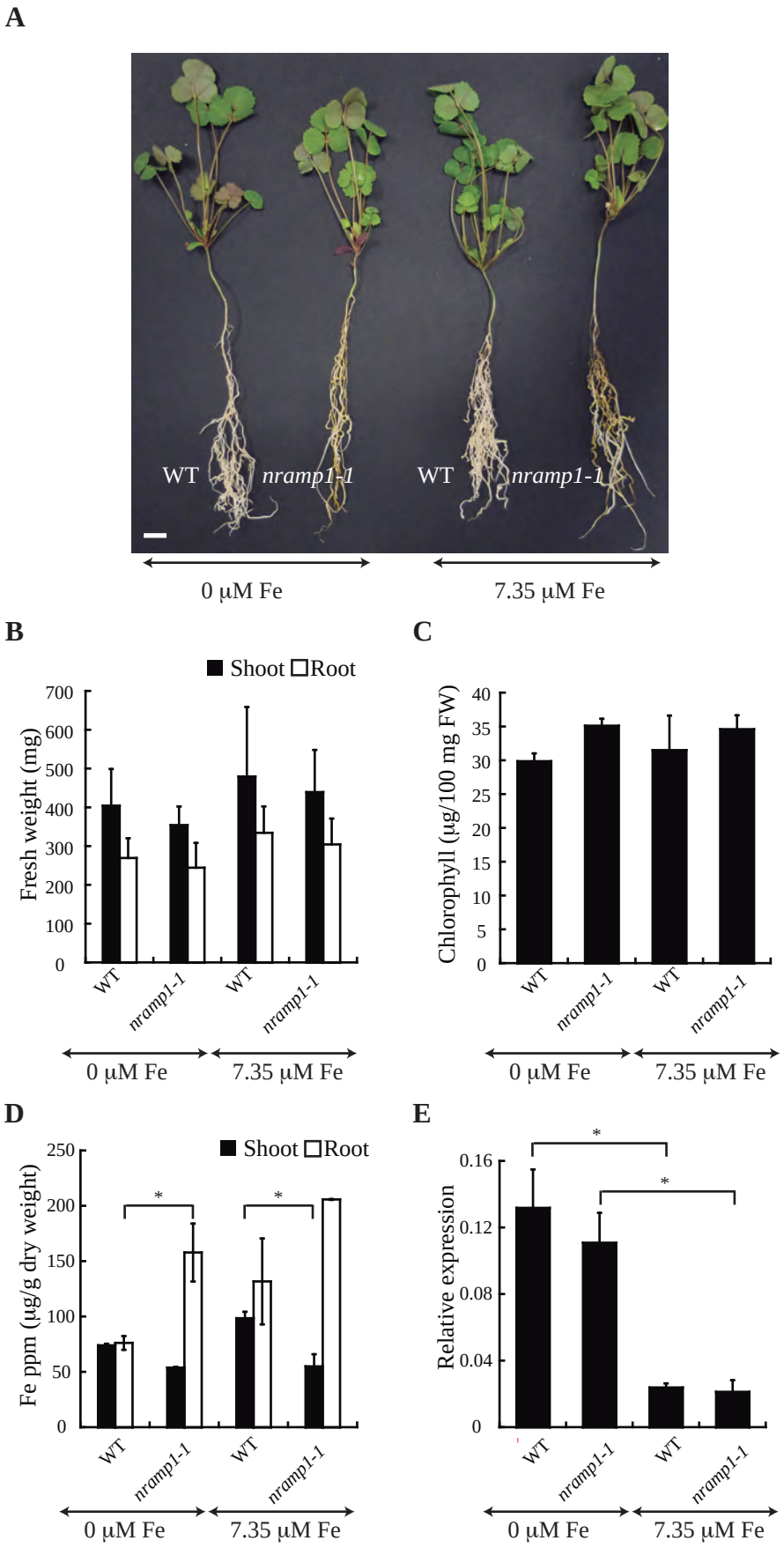

Supplemental Figure S6. Phenotype of *nramp1-1* under non-symbiotic conditions. (A) Growth of representative plants. Scale bar represents 1 cm. Fe concentrations in nutritive solutions used are indicated below. (B) Fresh weight of shoots and roots. Data are the mean ± SE (n = 5 plants). (C) Chlorophyll content. Data are the mean ± SE (n = 3 plants). (D) Iron content in roots and shoots of wild-type and *nramp1-1* plants under two different iron fertilization levels. Data are the mean ± SE of two sets of five pooled plants. * indicates significative differences ($p \leq 0.05$). (F) *MtFRO1* expression in wild type and nramp1-1 plants under two different iron fertilization levels. Data are the mean ± SE of three independet experiments. * indicates significative differences ($p \leq 0.05$).

SUPPLEMENTAL FIGURE S7

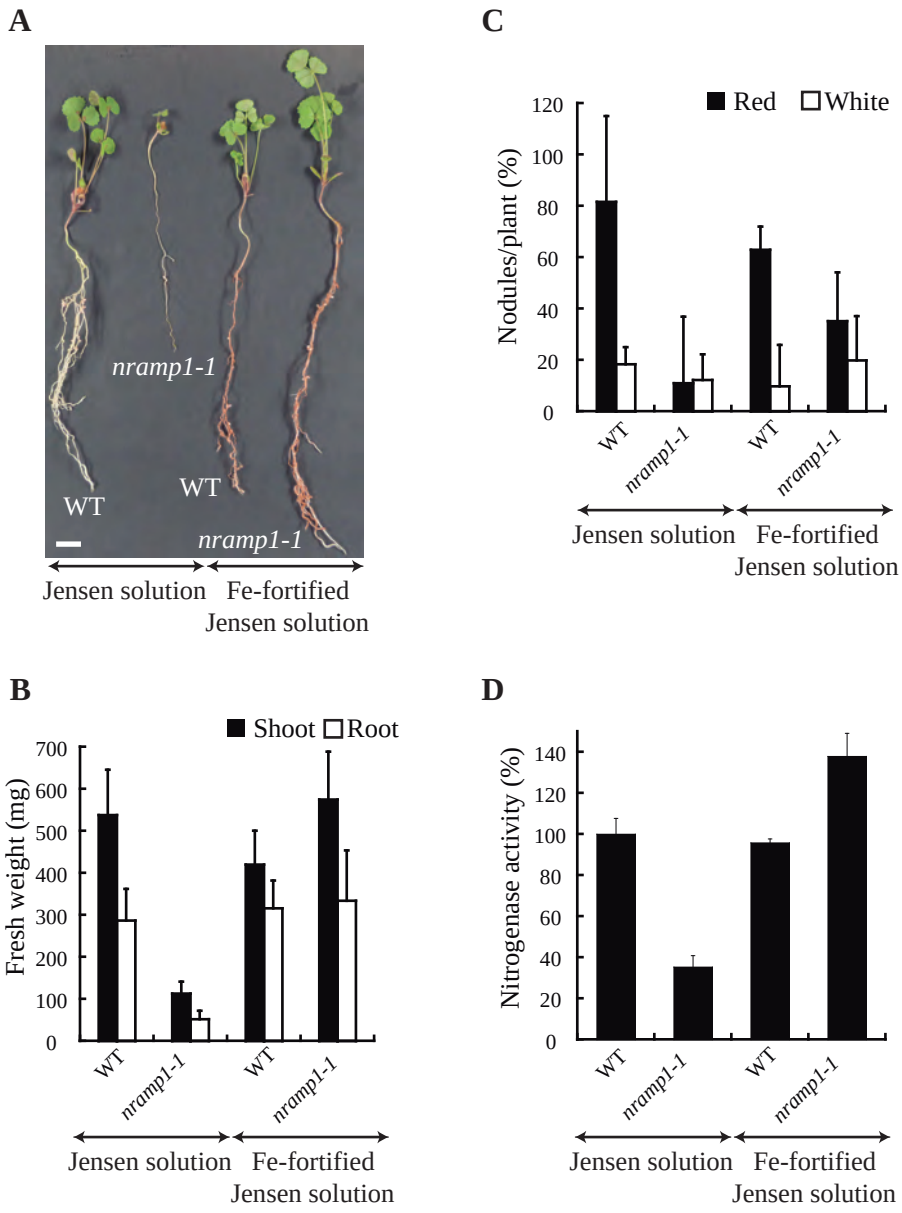

Supplemental Figure S7. Iron complementation of *nramp1-1* phenotype. (A) Growth of representative plants. Scale bar represents 1 cm. (B) Fresh weight of shoots and roots. Data are the mean ± SE (n = 8 plants). (C) Nodule number per plant. 100 % = 4.25 nodules/plant. Data are the average ± SE (n=8-10 plants). (D) Nitrogenase activity in 28 dpi nodules. Acetylene reduction was measured in duplicate from two sets of five pooled plants. Data are the mean ± SE. 100% = 61.17 nmol ethylene $h^{-1}g^{-1}$.

SUPPLEMENTAL FIGURE S8

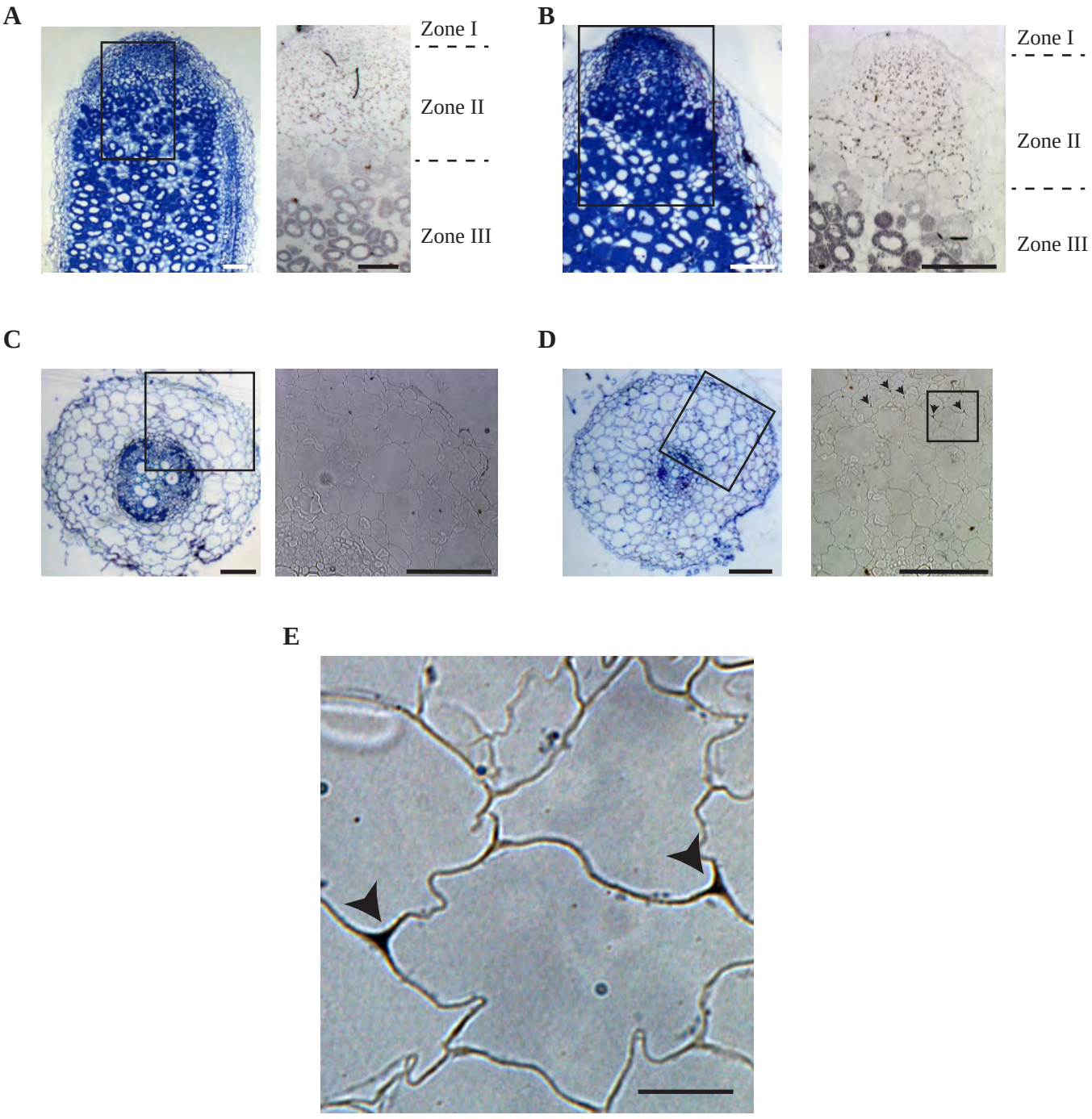

Supplemental Figure S8. Iron distribution in roots and nodules of wild type and *nramp1-1* plants. (A) wild type *M. truncatula* nodule and (B) *nramp1-1 M. truncatula* nodule. Left panels show reference sections stained with toluidine blue and methylene blue, the boxed regions represent the approximate area corresponding to the Perl-DAB-stained (right panel) which shows the iron distribution. Nodule zones are indicated. (C) Iron distribution in wild type *M. truncatula* root. Left panel shows a root section stained with toluidine blue and methylene blue, the boxed region represents the approximate area corresponding to the Perl-DAB-stained right panel. (D) Iron distribution in *nramp1-1 M. truncatula* root. Left panel shows a reference section stained with toluidine blue and methylene blue, the boxed region represents the approximate área corresponding to the Perl-DAB-stained right panel. Arrowheads indicate regions of iron accumulation. (E) Close-up view of Perl-DAB stained nramp1-1 root (corresponding to the boxed area of the right panel in D). Arrowheads indicate regions of iron accumulation. Scale bars represent 100 μm (A-C, and left panel D), 50 μm (right panel D), or 10 μm (E).

SUPPLEMENTAL FIGURE S9

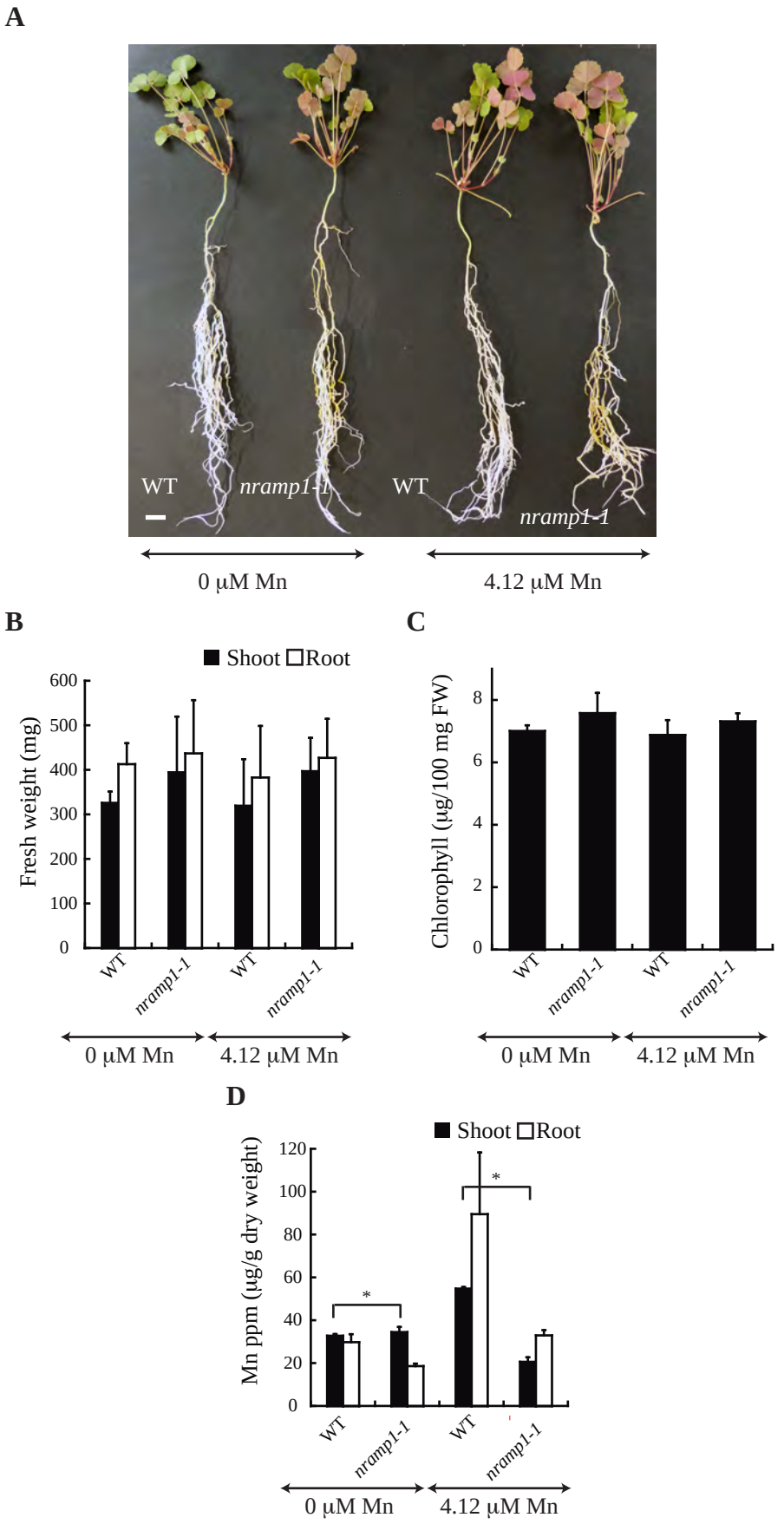

Supplemental Figure S9. Non-symbiotic phenotype of *nramp1-1* under Mn deficiency conditions. (A) Growth of representative plants. Scale bar represents 1 cm. Manganese concentrations in nutritive solutions used are indicated below. (B) Fresh weight of shoots and roots. Data are the mean ± SE (n = 5 plants). (C) Chlorophyll content. Data are the mean ± SE (n = 3 plants). (D) Manganese content in roots and shoots of wild-type and *nramp1-1* plants under two different manganes fertilization levels. Data are the mean ± SE of two sets of five pooled plants. * indicates significative differences ($p \leq 0.05$).

SUPPLEMENTAL FIGURE S10

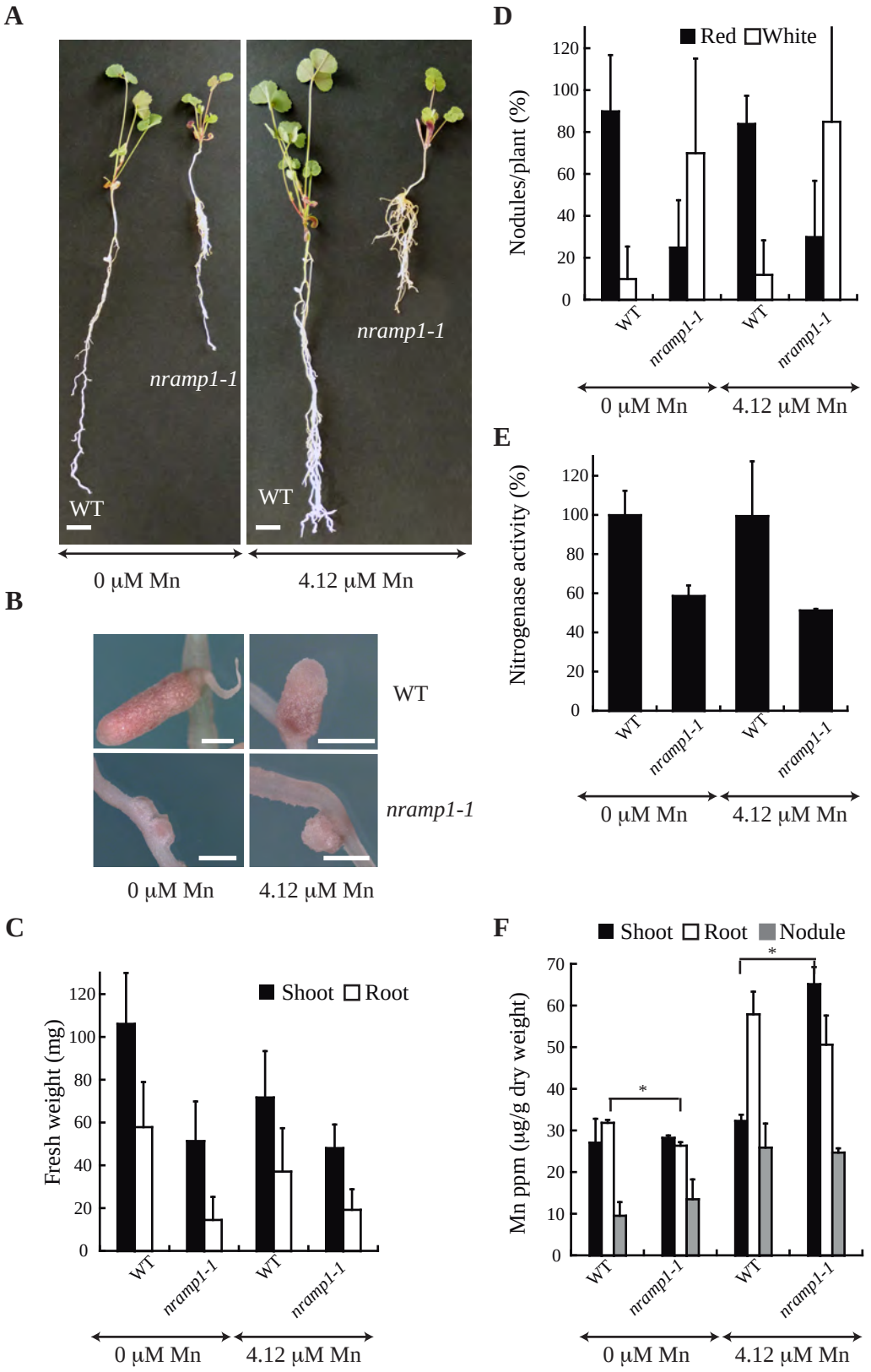

Supplemental Figure S10. Symbiotic phenotype of *nramp1-1* under two different Mn concentrations (A) Growth of representative plants. Scale bar represents1 cm. (B) Close view of representative nodules of each *M. truncatula* line. Scale bar represents 1 mm. (C) Fresh weight of shoots and roots. Data are the mean ± SE (n = 6-8 plants). (D) Nodule number per plant. 100 % = 4.21 nodules/plant. Data are the average ± SE (n= 7 plants). (E) Nitrogenase activity in 28 dpi nodules. Acetylene reduction was measured in duplicate from two sets of five pooled plants. Data are the mean ± SE. 100% = 26.69 nmol ethylene $h^{-1}g^{-1}$. (F) Mn content (ppm) in 28 dpi plants. Bars indicate the average ± SE of two sets of 5 transformed plants. * indicates significant differences ($p \leq 0.05$).